Reduced Reference Evapotranspiration and Aridity from 0.5°C Less Warming in the Yellow River Basin, China

Dongnan Jian[1, 2], Zhuguo Ma[1, 2], Daniel Mitchell[3], Liang Chen[1], Jianping Duan[1], Haoxin Zhang[1, 2], Ziyan Zheng[1], Meixia Lv[1]

[1] CAS Key Laboratory of Regional Climate-Environment for Temperate East Asia, Institute of Atmospheric Physics, Chinese Academy of Sciences, Beijing, China,

[2] University of Chinese Academy of Sciences, Beijing, China

Corresponding author: Zhuguo Ma (mazg@tea.ac.cn)

[3]School of Geographical Sciences, University of Bristol, Bristol, UK

Key Points:

- Changes in the reference evapotranspiration and aridity in the Yellow River Basin in response to warmings of 1.5°C and 2°C were quantified
- Compared to the reference period, the reference evapotranspiration and aridity increases in the 1.5 and 2 °C warmer worlds
- The reference evapotranspiration and aridity are lower in a 1.5 °C warmer world than in a 2 °C warmer world

Abstract

In this study, the reference evapotranspiration (ETo) in the Yellow River Basin (YRB) during 1961–2017 was calculated by the Penman-Monteith method from observed meteorological data, and the simulated ETo in the reference period (2006-2015) and with global warming levels of 1.5 and 2°C were calculated from the outputs of the Half a degree Additional warming, Prognosis and Projected Impacts (HAPPI) project. We found that the ETo increased significantly during 1961-2017 in the central and southern parts of the upper basin and western part of the middle basin, and it decreased significantly in the northeastern portion of the upper basin and the eastern portion of the middle basin and lower basin. The multiyear average ETo of the YRB projected by CAM4-2degree, ECHAM6-3-LR, MIROC5 and NorESM1-HAPPI increases by 49.1, 41.0, 30.9 and 47.6 mm at 1.5°C warming, respectively, and 77.9, 76.6, 93.7 and 80.6 mm at 2°C warming, respectively, compared to the reference period. The increment in the ETo exceeds the increment of the precipitation in warmer worlds. This phenomenon is likely to intensify the aridity in the YRB, especially at 2°C warming world. Limiting global warming to 1.5°C is the most beneficial to the North China Plain, southern part of Hetao Plain and Ordos Plateau and northwestern part of the Loess Plateau that ETo can be reduced over 30mm in these regions. The main factors contributing to the increase in ETo at the two warming levels are the maximum temperature (tasmax), downwelling shortwave radiation (rsds), and relative humidity (hurs).

1 Introduction

The Yellow River Basin (YRB) has played a significant role in China's long history, food production, and socioeconomic development (Cai and Rosegrant, 2004; Zhu et al., 2004). It has been reported that drought has occurred frequently in the YRB and has had socioeconomic and environmental effect (She and Xia, 2013). The drought that extended from the late 1920s to the early 1930s impacted approximately 20 million people and led to over 3 million deaths (Xie and Fu, 2004). The water crisis of the YRB has come into notice worldwide, especially the serious drying up of the main river in the lower basin that occurred during the 1990s (Cong et al., 2009). The drying up recorded at the Lijin station first started in 1972 and 20 instances of the river drying up occurred between this year and 1997. The most serious instance happened in 1997, when the area along the lower reaches dried up for 226 days over a distance of 704 km (Ma, 2005). In addition, both the observed and natural runoffs of the Yellow River showed decreasing trends during the last half century (Cong et al., 2009; Cuo et al., 2013; Wang et al., 2013; Yan et al., 2013; Yang et al., 2004) due to significant increases in the artificial water consumption (Cong et al., 2009; Wang et al., 2016; Yang et al., 2004). The water utilization for agriculture, industry, and households in the past decade seriously impacted the environmental and ecological water requirements (Cai and Rosegrant, 2004; Shiau et al., 2007; Zhu et al., 2004). With the growing economy and increasing population, the irrigation areas also progressively expanded from 800 thousand hectares in 1949 (Fu et al., 2004) to 4424 thousand hectares by 2007 (YRCC, 2007). The reference evapotranspiration (ETo) is

a good proxy to measure the drought conditions in environmental, hydrological and agricultural systems (Sun et al., 2015; Trenberth et al., 2013; Vicente-Serrano et al., 2012, 2015). An increase in evapotranspiration could have serious repercussions on water resources (McVicar et al., 2007). It has been proven that the most sensitive climate factor for naturalized streamflow in the YRB is the potential evapotranspiration (Lv et al., 2018). Its estimation and projection are thus crucial to understanding the water cycle of a basin or region (Jian et al., 2018; Su et al., 2017).

The evapotranspiration from a reference surface that is not short of water is the reference evapotranspiration. The reference surface is a hypothetical grass reference crop with an assumed crop height of 0.12 m, a fixed surface resistance of 70 s m-1 and an albedo of 0.23 (Allen et al., 1998). The reference surface is very similar to an extensive surface of green, well-watered grass of uniform height, actively growing and completely shading the ground (Allen et al., 1998). The ETo is an important parameter for the characterization of the hydrological cycle and is affected only by climatic parameters (Allen et al., 1998). It indicates an upper limit for the actual evapotranspiration in a humid climate, while it denotes the total available energy for actual evapotranspiration in an arid climate (Gong et al., 2006). It is the most important factor to consider in calculating the actual evapotranspiration (Wang et al., 2017; Xu and Singh, 2004). It is also an input to irrigation system and hydrological models and is important for the assessment of the hydrological impact of climate change (Xu et al., 2006). With climate warming, it was expected that the evapotranspiration will also increase (Roderick and Farquhar, 2002). However,

declines in the observed pan evaporation and ETo have been observed in many regions around the world by a great deal of studies, for example, in the United States and the former Soviet Union (Golubev et al., 2001; Peterson et al., 1995), India (Bandyopadhyay et al., 2009; Chattopadhyay and Hulme, 1997; Jhajharia et al., 2009), China (Liu et al., 2004), Australia (Roderick and Farquhar, 2004), Japan (Jun et al., 2004), and the Canadian Prairies (Burn and Hesch, 2007). Such a contrast between the expectation and observation is called the "evaporation paradox" (Roderick and Farquhar, 2002). Explanations for this phenomenon included the decreasing solar radiation or sunshine duration (Jhajharia et al., 2009; Liu et al., 2004; Peterson et al., 1995; Roderick and Farquhar, 2002; Xu et al., 2006) and wind speed (Burn and Hesch, 2007; Roderick et L., 2007), increasing relative humidity (Bandyopadhyay et al., 2009; Chattopadhyay and Hulme, 1997), and the complementary relationship between the actual and potential evapotranspiration (Hobbins, 2004). Some researchers found that the ETo increased in some areas of the upper and middle basins of YRB (Liu et al., 2010; Wang et al., 2012). The ETo is also projected to increase over the 21st century on the Loess Plateau (Li et al., 2012). Methods for the quantification of the ETo in a basin or region at specific warming targets are lacking. The issue of how the ETo will change in a warmer world and therefore give rise to drier or wetter conditions in the YRB is worth discussion due to its great socioeconomic impact.

The Paris Agreement was adopted on the 12th of December 2015 at the United Nations Framework Convention on Climate Change (UNFCCC) and provides a

framework for global actions to address climate change. The 2015 Paris Agreement reflected a commitment to "holding the increase in the global average temperature to well below 2.0 °C above pre-industrial levels and pursuing efforts to limit the temperature increase to 1.5 °C, recognizing that this would significantly reduce the risks and impacts of climate change". Since the Paris Agreement, there has been a call for assessing the effects from global warming of 1.5 and 2 °C (Mitchell et al., 2016; Schleussner et al., 2016). An IPCC special report on the impacts of global warming of 1.5 °C suggested that the climate-related risks in natural and human systems are lower for a global warming of 1.5°C than for 2°C (IPCC, 2018). Most published results have been based on the existing Coupled Model Intercomparison Project (CMIP5) (Taylor et al., 2012), which was not specifically designed for the assessment of the 1.5 and 2°C warming worlds (Mitchell et al., 2016). For that reason, HAPPI was proposed to provide a framework to assess the impacts at the 1.5°C warming level and the impacts avoided compared to those at 2°C (Mitchell et al., 2017). Researchers assessed changes in the runoff and water resources (Zhai et al, 2018), agricultural impacts (Ruane et al., 2018; Schleussner et al., 2018), climate extreme (Baker et al., 2018; Lewis et al, 2017; Seneviratne et al., 2018; Wehner et al., 2018), land–climate feedbacks and land-use forcing (Seneviratne et al., 2018) for global warming levels of 1.5 and 2 °C by using HAPPI outputs, but there has been limited discussion on the impacts of specific warming targets on a region or basin.

Here, the ETo of the YRB from 1961 to 2017 was calculated by Penman-Monteith equation based on observed meteorological data. We evaluated the

simulations of HAPPI of the ETo by comparing the multiyear average and spatial pattern of the ETo. Using the HAPPI outputs, we examine how much the ETo may change under stabilized global mean temperature increases of 1.5 and 2°C above preindustrial levels in the YRB and estimate the beneficial reduction that will be achieved by limiting global warming to 1.5°C, focusing on the potential changes of aridity. We calculate the relative contributions of climatic variables to the change in ETo at two warming levels. The results are expected to contribute to an understanding of the regional patterns in ETo under two global warming levels.

2 Materials and Methods

2.1Study area

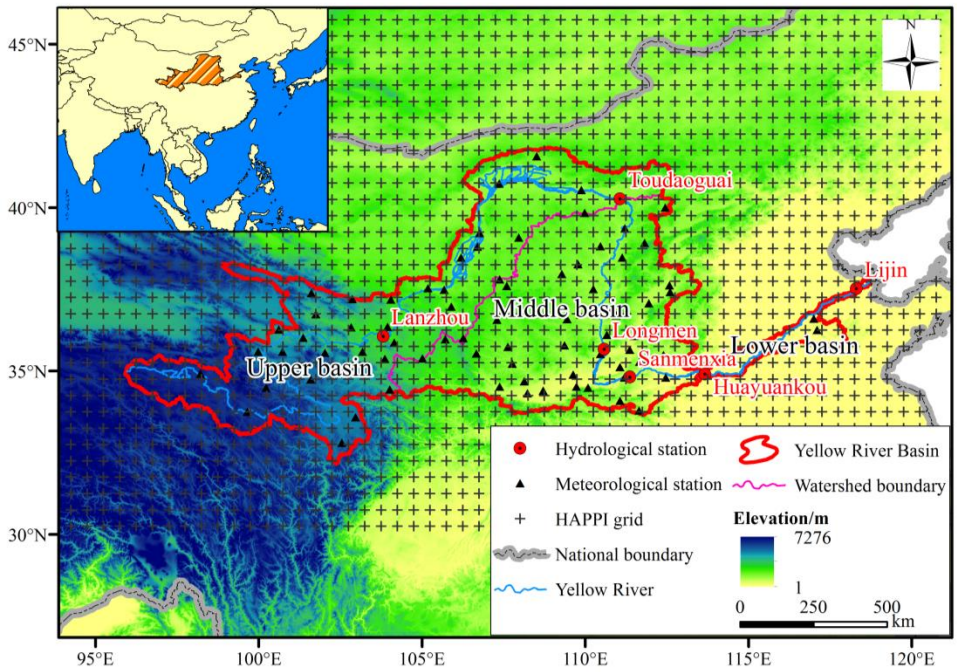

Fig. 1. Location of the YRB and its subbasin as well as of the hydrological and meteorological stations and the HAPPI grid

The Yellow River (Fig. 1), originating from the Qinghai-Tibet Plateau, is the second-longest river in China, with a length of 5464 km, and it covers a drainage area of 79.5×104 km^2 (YRCC., 2015). The YRB supports a population of approximately 110 million people and has 12.6×106 ha of cultivated land (Shiau et al., 2007). From northwest to southeast, the climate of the YRB is characterized by an arid, semiarid continental monsoon climate and semi-humid climate (Wang and Peng, 2017). The YRB covers three typical landforms, namely, the Tibetan Plateau (2000-5000 m), the Loess Plateau (500-2000 m), and the alluvial plain (Yang et al., 2004). The tributaries upstream of Lanzhou station flow into the main channel of the Yellow River and account for 62% of the runoff of the whole basin (Wang and Peng, 2017). There is a slow-flowing stream from Lanzhou to Toudaoguai stations, and the basin valley and Hetao Plain are located in this section. Downstream of Toudaoguai station, the Yellow River flows through the Loess Plateau, where there is serious water loss and soil erosion, and 90% of the sediment delivered to the Yellow River comes from here (Tang et al., 1991). “Revegetation schemes” and “engineering methods” were used to reduce the sediment loads reaching the Yellow River (McVicar, 2007). From Sanmenxia to Huayuankou stations, the river has many tributaries, and the slope of river is steep, helping the production of runoff and confluence. Downstream of Huayuankou station is the North China Plain. Large quantities of sediment are carried by mudflow from the plateau and cause serious silting and aboveground rivers in the lower reaches (Douglas, 1989; Shi and Shao, 2000). Issues of water shortages and environmental deterioration have become very serious in the YRB and the prime

water-related issues in this basin are soil erosion and sedimentation, flooding, and water shortages (Wang and Peng, 2004). Flooding and drought have negatively impacted the agriculture and people's lives in the lower basin and caused huge economic losses and human death and injury (Wang and Peng, 2017).

2.2 Data

In current study, daily observed data from 80 meteorological stations (Fig. 1) in the YRB during the period of 1961-2017, including the air temperature, precipitation, maximum /minimum air temperature, relative humidity, atmospheric pressure, wind speed (10-m height), and sunshine duration, were obtained from the National Meteorological Information Center of the China Meteorological Administration. The data quality was checked by means of climatic boundary values, extreme values, and internal consistency. Stations missing more than 5% of the days in a year were rejected. The missing daily records of a station were filled by the multiyear averaged values of the station.

The discharge data in this study included naturalized and observed streamflows at a total of 6 hydrological stations (Fig. 1). Annual data were available from 1961 to 2010 for the Lanzhou, Toudaoguai, Longmen, Sanmenxia, Huayuankou and Lijin stations. Annual data were obtained from the Yellow River Conservancy Commission, which is the sole authority in China in charge of quality control and the release of water data (Fu et al., 2004). Given the intense human activities in the YRB, naturalized streamflow data without human intervention were also considered in the

183 current study. The naturalized and observed streamflows are different in their
184 influence from human activities, such as reservoir regulation, interbasin water
185 diversion, and water withdrawal for irrigation, industrial, and domestic uses (Fu et al.,
186 2004; Lv et al., 2017). The locations of the meteorological stations, the hydrological
187 stations, and the subbasins are shown in Fig. 1.

188 The climate output data used in this study are projections from the Half a
189 degree Additional warming, Projections, Prognosis and Impacts project (HAPPI;
190 Mitchell et al., 2017). HAPPI provides climate data to assess how the climate,
191 especially extreme weather, might be different from the present in the world under
192 conditions 1.5 and 2.0°C warmer than pre-industrial conditions (Mitchell et al., 2017).
193 HAPPI is based on the atmospheric components of CMIP5 models forced by
194 prescribed sea surface temperature (SST) and sea ice concentrations (Mitchell et al.,
195 2017). Four GCMs (Tab. 1), CAM4-2degree, ECHAM6-3-LR, MIROC5, and
196 NorESM1-HAPPI, were used in the current study and were bias-corrected using the
197 Inter-Sectoral Impact Model Intercomparison Project (ISIMIP2b) (Lange, 2018). The
198 bias correction was applied to each ensemble members of each of the four HAPPI
199 GCMs and has significantly improved the ensemble mean performance while
200 preserving the ensemble variability (Döll et al., 2018). The reference period of the
201 HAPPI experiment is the most recent decade from 2006–2015. The 1.5 and 2°C
202 warmer than pre-industrial (1861-1880) experiment is based on the RCP2.6
203 experiment from 2106 to 2115 and the weighted combination of the RCP2.6 and
204 RCP4.5 experiments from 2106 to 2115, respectively. The model outputs include the

205 air temperature (tas), maximum (tasmax)/minimum air temperature (tasmin), relative
206 humidity (hurs), wind speed (sfcWind), precipitation (prec), and downwelling
207 shortwave (rsds)/ longwave radiation (rlds).

208 Tab. 1. Details of the HAPPI models used in this study. Note the horizontal resolution was
209 changed from the modal native resolution during the ISI-MIP bias correction method.

GCM	Ensemble members: allhist/plus1.5/plus2.0	Horizontal Resolution
CAM4-2degree	20/20/20	0.5°×0.5°
ECHAM6-3-LR	20/20/20	0.5°×0.5°
MIROC5	10/10/10	0.5°×0.5°
NorESM1-HAPPI	20/20/20	0.5°×0.5°

210 2.3Method

211 The Penman–Monteith method was applied in the current study to calculate
212 the ETo. It has been recommended by the Food and Agricultural Organization (FAO)
213 as the best method to determine the ETo (Allen et al., 1998).

214 $$ET_o = \frac{0.408\Delta(R_n - G) + \gamma \frac{900}{T+273} u_2(e_{s-}e_a)}{\Delta + \gamma(1 + 0.34u_2)} \quad (1)$$

215 where Rn represents the net radiation at the crop surface (MJ m-2 day-1), G is
216 the soil heat flux density (MJ m-2 day-1), u2 is the wind speed at a 2 m height (m s-
217 1), e_s is the saturation vapor pressure (kPa), ea is the actual vapor pressure (kPa), $e_s - e_a$
218 is the saturation vapor pressure deficit (kPa), Δ is the slope vapor pressure curve
219 (kPa °C-1), and γ is a psychrometric constant (kPa °C-1). The daily soil heat flux is
220 regarded as 0 in the current study (Allen at al., 1998).

Detailed algorithms of the above variables were according to Allen at al. (1998). Observed meteorological factors, including the maximum/minimum air temperature, relative humidity, atmospheric pressure, sunshine duration, and wind speed, were used to calculate the ETo. HAPPI outputs, including the tasmax, tasmin, hurs, sfcWind and rsds, were involved in computing the ETo. In the current study, the air temperature was computed as the average of the tasmax and tasmin, as was recommend by the FAO (Allen et al., 1998). The HAPPI outputs do not include the atmospheric pressure and the sunshine duration, which are necessary to calculate the psychrometric constant and net radiation. The effect of the atmospheric pressure is small in the calculation of the ETo (Allen at al., 1998). A simplification of the ideal gas law, assuming 20°C for a standard atmosphere, was used to calculate P (Allen at al., 1998):

$$P = 101.3(\frac{293 - 0.0065z}{293})^{5.26} \qquad (2)$$

Where P is the atmospheric pressure (kPa) and z is the elevation above sea level (m).

HAPPI provides the rsds and rlds data, but it does not have upwelling longwave radiation data. We used the following equations to calculate the net radiation. The net shortwave radiation R_{ns} is expressed in the follow equation:

$$R_{ns} = (1 - \alpha)R_s \qquad (3)$$

Where R_{ns} is the net solar or shortwave radiation (MJ m^{-2} day^{-1}), α is the albedo or canopy reflection coefficient, which is 0.23 for the hypothetical grass

reference crop (dimensionless), and $R_s$is the downwelling solar radiation (MJ m^{-2} day^{-1}).

The extraterrestrial radiation R_a can be estimated from the solar constant, the solar declination and the time of the year by:

$$R_a = \frac{12(60)}{\pi} G_{SC} d_r [\omega_S \sin(\varphi)\sin(\delta) + \cos(\varphi)\cos(\delta)(\sin(\omega_s))] \quad (4)$$

Where R_a is the extraterrestrial radiation (MJ m^{-2} day^{-1}), G_{SC} is the solar constant = 0.0820 MJ m^{-2} min^{-1}, d_r is the inverse relative Earth-Sun distance (Equation 5), δ is the solar declination (Equation 6) (rad), ω_s is the sunset hour angle (Equation 7) (rad), and φ is the latitude (rad).

The inverse relative Earth-Sun distance (d_r), the solar declination (δ) and sunset hour angle (ω_s) are given by:

$$d_r = 1 + 0.033cos\left(\frac{2\pi}{365}J\right) \quad (5)$$

$$\delta = 0.409\sin\left(\frac{2\pi}{365}J - 1.39\right) \quad (6)$$

$$\omega_s = arccos[-tan(\varphi)tan(\delta)] \quad (7)$$

Where *J* is the number of the day in the year between 1 and 365 or 366.

$$R_{nl} = \sigma\left[\frac{T_{max,K}^4 + T_{min,K}^4}{2}\right]\left(0.34 - 0.14\sqrt{e_a}\right)\left(1.35\frac{R_s}{R_{so}} - 0.35\right) \quad (8)$$

Where R_{nl} is the net outgoing longwave radiation (MJ m^{-2} day^{-1}), σ is the Stefan-Boltzmann constant (4.903×10^{-9} MJ K^{-4} m^{-2} day^{-1}), $T_{max,K}$ is the maximum absolute temperature during the 24-hour period (K = °C + 273.16), $T_{max,K}$ is the minimum absolute temperature during the 24-hour period (K = °C + 273.16), e_a is the actual vapor pressure (kPa), R_s/R_{so} is the relative shortwave radiation (limited to ≤1.0), and R_{so} is the clear-sky radiation (Equation 9) (MJ m^{-2} day^{-1}).

The calculation of the clear-sky radiation (R_{so}) is as follows:

$$R_{so} = (0.75 + 2 \times 10^{-5} z) R_a \quad (9)$$

Where z is the station elevation above sea level (m).

The net radiation (R_n) is the difference between the incoming net shortwave radiation (R_{ns}) and the outgoing net longwave radiation (R_{nl}):

$$R_n = R_{ns} - R_{nl} \quad (10)$$

To characterize the average difference between the ETos estimated by the observed and simulated data at a grid point or region, the mean error (BIAS) is estimated, which is defined as the positive or negative difference between the observed (o) and simulated (s) means of the indicator. The equation for the BIAS is given here:

$$BIAS = \frac{1}{n} \sum_{i=1}^{n} (s_i - o_i) = \overline{s} - \overline{o} \quad (11)$$

To quantify the contribution of a climatic variable to the change of ETo at 1.5 and 2°C warming levels, a simple but practical method was employed as follows. Taking 1.5°C warming as an example, (1) a climatic variable at the reference period and other climatic variables at 1.5°C warming were considered to recalculate the ETo; (2) the recalculated and original ETos at the 1.5°C warming level were compared and (3) the difference was regarded as the influence of the change at 1.5°C warming by that variable. The same method was applied to determine the contribution of a climatic variable to the change of the ETo at 2°C warming level.

284 We used linear regression to analyze the trends in the climatic variables and
285 the nonparametric and Mann–Kendall (MK) test (Kendall, 1975; Mann, 1945) to
286 assess the significance. Inverse distance weighted (IDW) was used to interpolate the
287 ETos in meteorological stations to the same grid as HAPPI to evaluate the
288 performance of HAPPI on ETo. We assessed the relationships between the variables
289 by using Pearson correlation coefficients.

290 **3 Results**

291 3.1 Climatic and hydrologic characteristics

292 To have a comprehensive understanding of the long-term variability in the
293 climate and river discharge of the YRB, the annual average temperature and
294 precipitation and decadal average of the river discharges were examined. The YRB
295 has become increasingly warmer over the last 5–6 decades, in where the average air
296 temperature has increased at a rate of 0.035±0.0031°C yr^{-1} ($p<0.05$) during the period
297 of 1961-2017 (Fig. 2(a)). Especially in the upper basin, it has experienced an
298 increasing rate of 0.030±0.0033°C yr^{-1} ($p<0.05$). The air temperature has increased at
299 a rate of 0.027±0.0038°C yr^{-1} and 0.019±0.0039°C yr^{-1} ($p<0.05$) for the middle and
300 lower basins, respectively. Over the analysis period, the areal averaged precipitation
301 was highest in the lower basin (precipitation =881.3 mm), followed by the middle
302 basin (precipitation=521.8 mm), and upper basin (precipitation = 347.5 mm) (Fig. 2
303 (b)).

The precipitation of the YRB showed a slight decreasing trend, but the change is not significant. The areal average precipitation is approximately 461.3 mm for the whole basin. Overall, the precipitation for the whole, upper, middle and lower basins decreased at rates of 0.40±0.49, 0.09±0.41, 0.66±0.63 and 0.90±1.82 mm yr^{-1}, respectively, from 1961 to 2017.

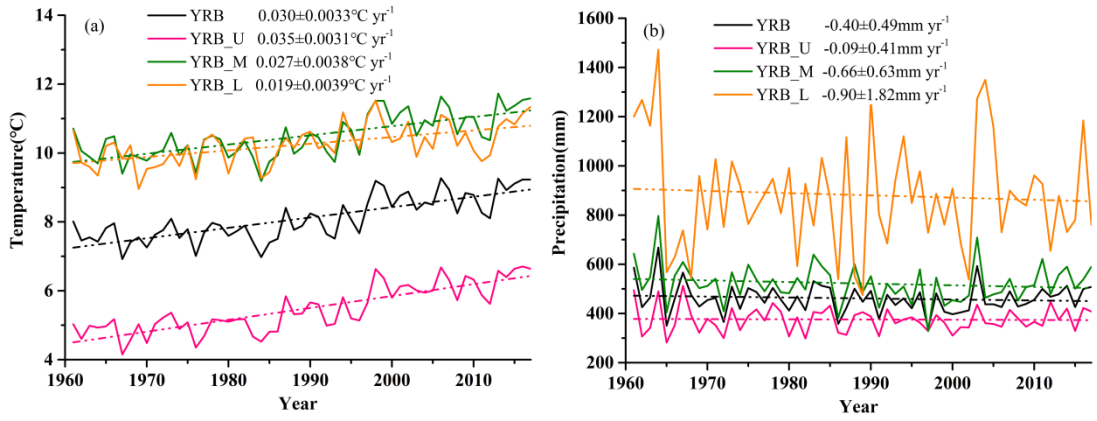

Fig. 2. Time series of: (a) annual temperature and (b) annual precipitation in the whole (black line), upper (pink line), middle (green line) and lower (orange line) basins from 1961 to 2017

Ma et al. (2005) found that the natural runoff in the YRB changed decadally. Both the observed and natural runoffs recorded at Lanzhou, Toudaoguai, Longmen, Sanmenxia, Huayuankou and Lijin stations have the same generally decreasing trend. The natural and observed runoffs showed decreasing trends at all stations, and the observed runoff decreased more obviously. The average of the natural runoff during the 2000s compared to the 1960s decreased by 14.5%, 14.9%, 15.2%, 18.0%, 19.0% and 19.0% for the Lanzhou, Hekou, Longmen, Sanmenxia, Huayuankou and Lijin stations, respectively. During the last 5 decades, except for Lijin station, the observed

321 runoffs showed their smallest changes between the 1960s and the 1980s and their
322 biggest changes from the 1990s to the 2000s. The runoff at Lijin station had a sharp
323 decreasing trend from the 1970s, and has declined unceasingly since the 1990s. The
324 averages of the observed runoff during the 2000s compared to the 1960s decreased by
325 23.3%, 43.8%, 47.9%, 56.0%, 53.6% and 70.5% for Lanzhou, Toudaoguai, Longmen,
326 Sanmenxia, Huayuankou and Lijin stations, respectively. Furthermore, as shown in
327 Tab. 2, the difference between the observed and natural runoffs became wider,
328 indicating there was a rapid increase in artificial water consumption, which
329 aggravated the water resource crisis of the YRB.

330 Tab. 2. Decadal averages of observed/natural runoffs (10^8 m^3)

	Lanzhou	Toudaoguai	Longmen	Sanmenxia	Huayuankou	Lijin
1961-1970	355.8/355.7	270.2/335.7	337.1/363.1	464.5/469.9	522.8/526.0	527.4/527.6
1971-1980	318.5/322.9	232.6/306.9	280.4/329.3	350.7/401.6	373.8/439.8	294.7/441.4
1981-1990	338.7/358.4	241.9/343.6	279.9/365.5	376.9/457.5	419.0/506.5	293.5/508.1
1991-2000	254.2/277.0	150.4/259.1	189.6/280.1	225.4/342.7	236.9/379.5	119.2/381.1
2001-2010	273.0/304.3	151.9/285.8	175.5/307.8	204.2/385.5	242.7/426.0	155.4/427.6
mean	308.1/323.6	209.4/306.2	252.5/329.2	324.3/411.4	359.0/455.5	278.0/457.1

331 ## 3.2 Observed ETo for the period 1961-2017

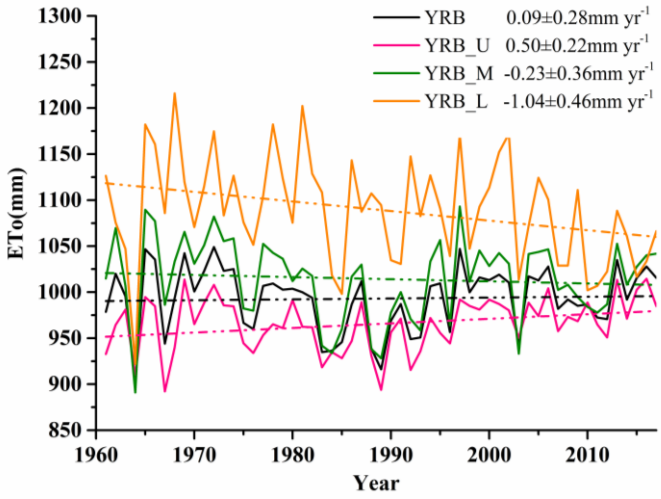

332

333 Fig. 3. Temporal variation of the annual ETo in the whole (black line), upper (pink line), middle

334 (green line) and lower (orange line) basins of the YRB from 1961 to 2017

335 The temporal trends for the annual ETo during the period of 1961-2017 in the

336 whole, upper, middle, and lower basins are shown in Fig. 3. The ETo in the whole and

337 upper basins showed increasing trends for the period from 1961 to 2017. There was a

338 significant ($p<0.05$) increasing trend at a rate of 0.50±0.22 mm yr^{-1} for the upper

339 basin, and the ETo had an increasing but insignificant trend with a rate of 0.09±0.28

340 mm yr^{-1} for the whole basin. The ETos in the middle and lower basins showed

341 significant ($p<0.05$) declining trends at rates of -0.23±0.36 and 1.04±0.46 mm yr^{-1},

342 respectively. The multiyear average ETos were approximately 993.0, 965.5, 1014.2,

343 and 1089.2 mm for the whole, upper, middle, and lower basins, respectively.

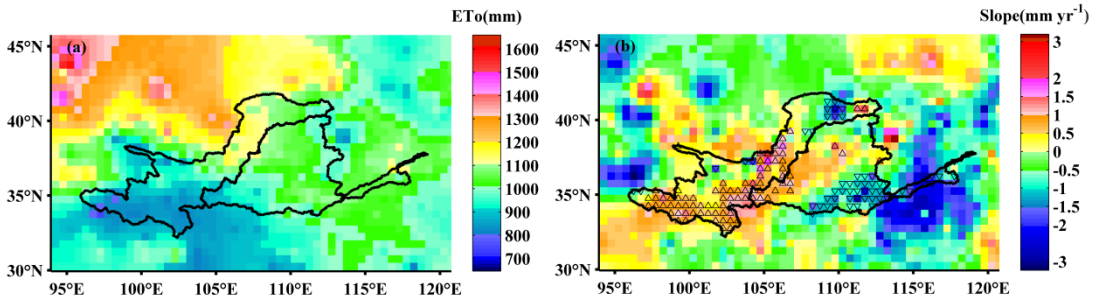

Fig. 4. (a) Spatial distribution of the annual ETo in the YRB from 1961 to 2017. (b) Annual trend slopes and the MK test result (at the 99% and 95% confidence levels) of the ETo during 1961–2017. The colorbar indicates the trend slope of the ETo. The red upward and blue downward triangles indicate significant (95% confidence) increasing and decreasing tendencies, respectively, according to the MK test.

The spatial distribution of the annual ETo over the YRB is shown in Fig. 4. (a). The high ETo values were mainly located in the northern region of the upper basin. In these regions, the annual ETos were mostly greater than 1100 mm. The ETo values in the southern part of the upper basin were relatively low. A large part of this area had an annual ETo less than or equal to 900 mm. The ETo values were between 900 and 1000 mm in the center of the upper basin and western region of the middle basin and between 1000 and 1100 mm in the eastern region of the middle basin and lower basin.

The spatial distribution of the ETo trends is presented in Fig. 4(b). The ETo increased in most areas of the upper and middle basins and showed decreasing trends throughout the lower basin, the eastern and some northern parts of the middle basin and the northeastern part of the upper basin. There were significant increasing trends ($p<0.05$) across wide areas in some of the central and southern parts of the upper

363 basin and the western part of the middle basin, where the ETo increased at over 0.5
364 mm yr^{-1}. The ETo decreased significantly ($p<0.05$) in a fraction of the northeastern
365 part of the upper basin, southeastern part of the middle basin and most of the lower
366 basin, where the reduction rate exceeded 0.5 mm yr^{-1}. It can be seen from the plot that
367 the ETo decreased most obviously in the lower basin, where the decreasing rate was
368 over 1.5 mm yr^{-1}.

369 3.3 Evaluation of HAPPI simulations

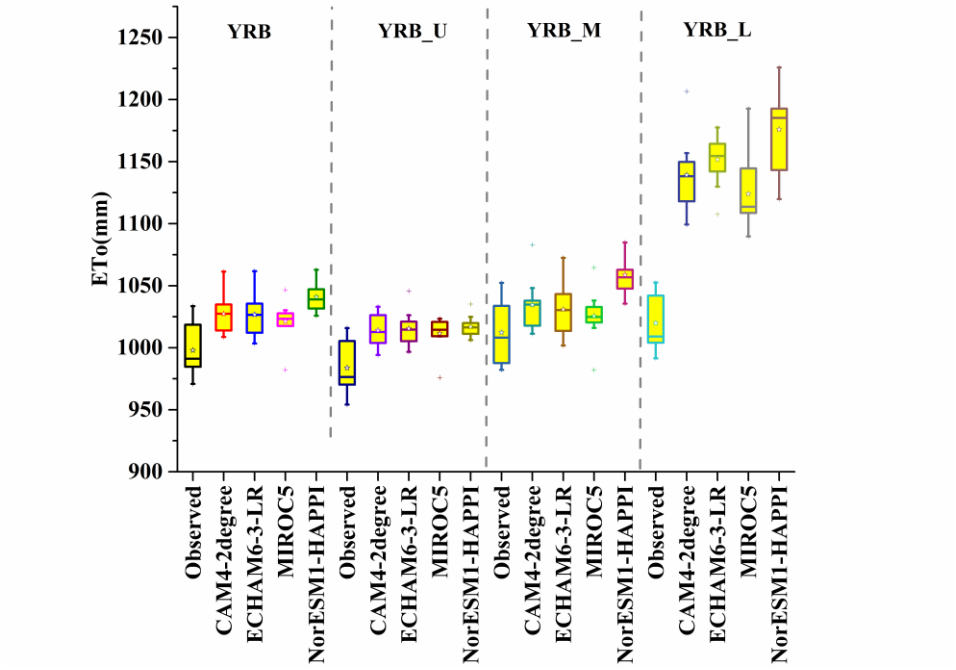

370

371 Fig. 5. Comparison of ETo calculated by observed data with ensemble mean ETo of mode
372 calculated by HAPPI in the whole (YRB), upper (YRB_U), middle (YRB_M) and lower (YRB_L)
373 basins during the reference period from 2006 to 2015. Horizontal lines in each boxplot represent
374 the 10 years' 1st and 25th percentiles, median, and 75th and 99th percentiles, respectively; the star
375 represents the mean ETo, and the plus signs represent the minimum and maximum.

376 The boxplots of the annual ETo based on the observations and simulations
377 from 2006 to 2015 in the whole, upper, middle and lower basins are shown in Fig. 5.
378 HAPPI has slightly higher simulation values for the ETo for the majority of the basin.
379 They give the best simulations of the ETo in the middle and upper basins and
380 relatively poor simulation in the lower basin. The biases of the multiyear average ETo
381 from the CAM4-2degree, ECHAM6-3-LR, MIROC5, and NorESM1-HAPPI were
382 29.4, 28.9, 23.6 and 43.2 mm for the whole basin, respectively, 30.5, 31.9, 28.0 and
383 33.4 mm for the upper basin, respectively, 22.2, 18.6, 13.3 and 46.4 mm for the
384 middle basin, respectively, and 119.2, 131.7, 104.0 and 156.1 mm for the lower basin,
385 respectively. Although the GCMs give the maximal bias for the ETo in the lower
386 basin, the lower basin is a very small part of the whole.

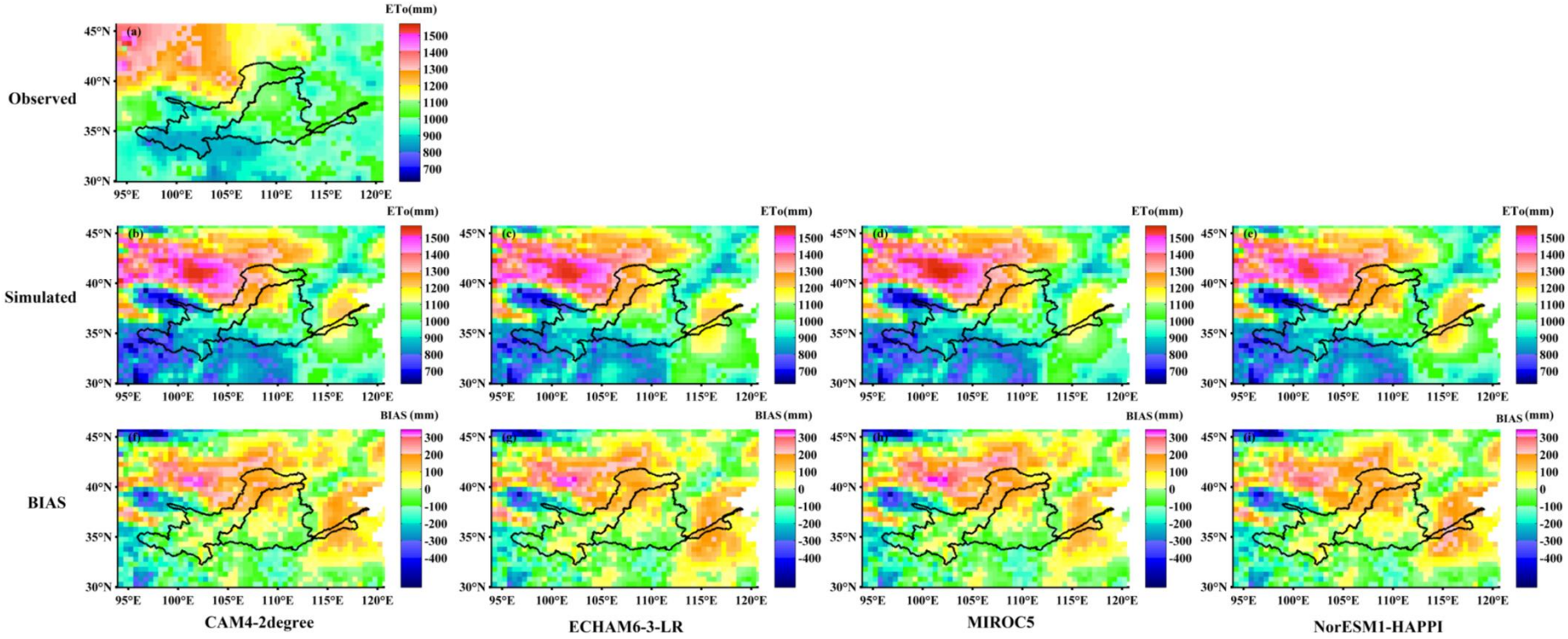

387

388 Fig. 6. Spatial patterns of the ETo estimated from: (a) observed and simulated data of (b) CAM4-2degree, (c) ECHAM6-3-LR, (d) MIROC5 and (e) NorESM1-

389 HAPPI and the difference between ETos calculated using simulated data of (f) CAM4-2degree, (g) ECHAM6-3-LR, (h) MIROC5 and (i) NorESM1-HAPPI and ETo

390 calculated using observed data during the period of 2006-2015.The simulated ETo were ensemble mean ETo of mode.

391 The spatial patterns of ETos estimated from observed and simulated data during 2006-
392 2015 are presented in Fig. 6 and were well simulated in the YRB. The spatial
393 distributions of the ETo from CAM4-2degree, ECHAM6-3-LR, MIROC5, and
394 NorESM1-HAPPI were similar to those of the ETo from observations, in which the
395 ETo was highest in the northern part of the upper basin, followed by the northwestern
396 part of the middle basin and the lower basin, the center of the middle basin, the
397 southern part of the middle basin and the center part of the upper basin. The ETos in
398 the southern part and west corner of the upper basin were also the lowest. The
399 correlation coefficients between the ETos calculated from observed data and from
400 CAM4-2degree, ECHAM6-3-LR, MIROC5, and NorESM1-HAPPI were 0.89, 0.89,
401 0.88 and 0.89, respectively, which is significant at the 99% confidence level.
402 However, HAPPI simulated higher ETos in the northern parts of both the upper and
403 middle basins and the lower basin, while a lower simulated ETo was obtained in some
404 southwestern parts of the upper basin and some southern parts of the middle basin.

405 ## 3.4 ETo for global warming of 1.5 and 2.0 °C

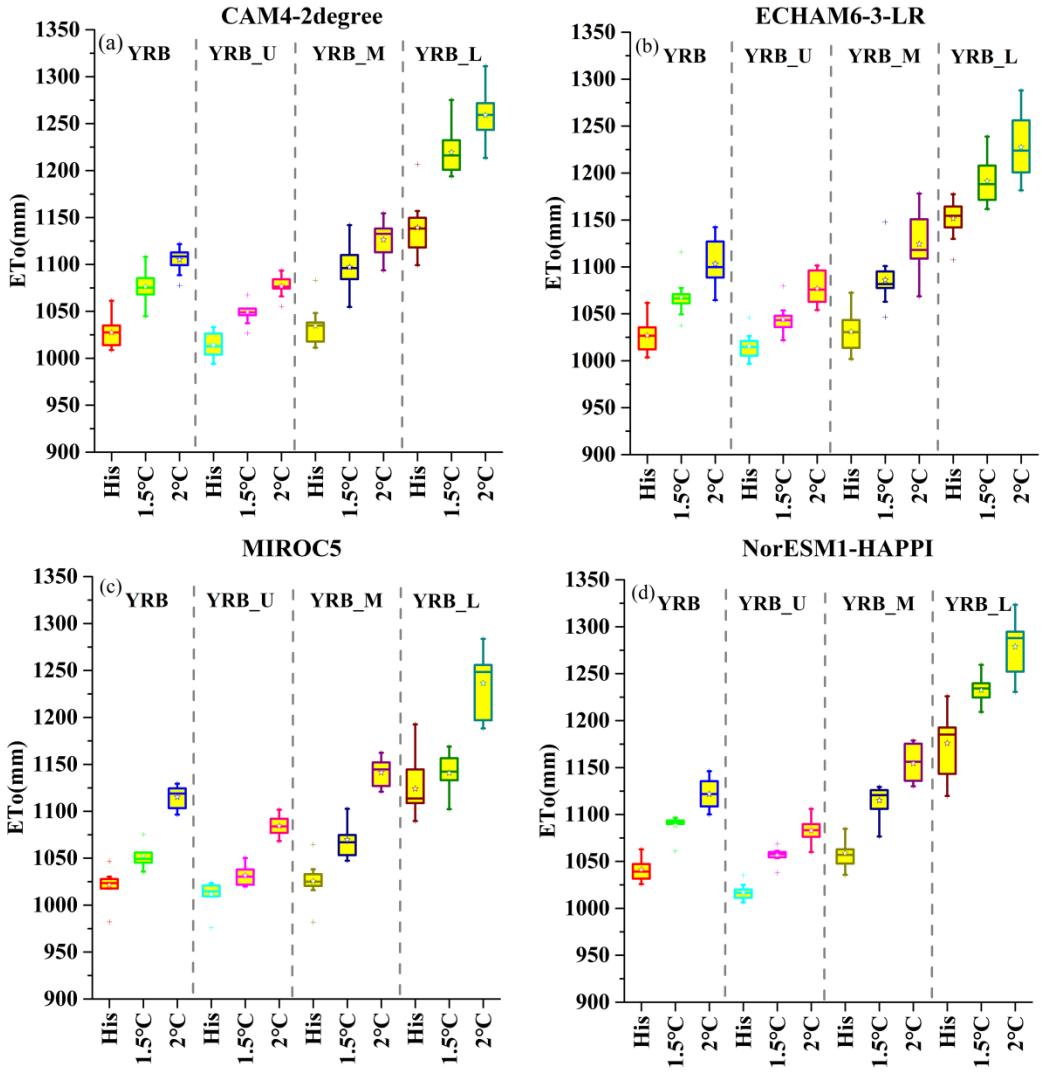

406

407 Fig. 7. Comparison of ensemble mean ETo of mode in the whole (YRB), upper (YRB_U), middle

408 (YRB_M) and lower (YRB_L) basins during the reference period from 2006 to 2015 and for the

409 1.5 and 2.0 °C for (a) CAM4-2degree, (b) ECHAM6-3-LR, (c) MIROC5, (d) NorESM1-HAPPI.

410 The boxplots of the ETo in the reference period and for the 1.5 and 2.0 °C

411 increases over pre-industrial levels are shown in Fig. 7. The ETo is projected to

412 increase at both the 1.5 and 2°C global warming levels compared to the period of

413 2005-2015 for each GCM. The increment of the ETo at the 2°C level is more than that

414 at the 1.5°C level. The ETo increases the most in the lower basin at both warming
415 levels. At the 1.5°C warming level, the multiyear average ETo increases by 49.1,
416 41.0, 30.9 and 47.6 mm in the whole basin for CAM4-2degree, ECHAM6-3-LR,
417 MIROC5 and NorESM1-HAPPI, respectively, compared to the reference period. The
418 increment of the multiyear average ETo in the upper basin is less than that in the
419 whole basin, and it reaches 35.1, 28.4, 20.0 and 39.4 mm for CAM4-2degree,
420 ECHAM6-3-LR, MIROC5 and NorESM1-HAPPI, respectively. The increments of
421 ETo for the CAM4-2degree, ECHAM6-3-LR, MIROC5 and NorESM1-HAPPI are
422 approximately 62.7, 55.1, 44.1, and 56.2 mm for the middle basin, respectively, and
423 80.2, 39.8, 16.8 and 56.4 mm for the lower basin. In the 2°C warming, the multiyear
424 average ETo for the CAM4-2degree, ECHAM6-3-LR, MIROC5 and NorESM1-
425 HAPPI increases by 77.9, 76.6, 93.7 and 80.6 mm for the whole basin, respectively,
426 62.7, 61.5, 72.8 and 65.8 mm for the upper basin, respectively, 91.9, 93.5, 115.7 and
427 95.7 mm for the middle basin, respectively, and 119.8, 75.8, 112.5 and 102.7 mm for
428 the lower basin, respectively.

429 Compared to a 1.5°C warmer world, the ETo increases most obviously in the
430 lower basin in the 2°C warmer world. The increment increases to 28.7, 35.6, 62.8 and
431 33.0 mm in the whole basin for CAM4-2degree, ECHAM6-3-LR, MIROC5 and
432 NorESM1-HAPPI, respectively, implying that increases in the ETo of approximately
433 28.7-62.8 mm can be avoided by limiting global warming to 1.5°C. The ETo
434 projected by CAM4-2degree, ECHAM6-3-LR, MIROC5 and NorESM1-HAPPI
435 increases by 27.6, 33.1, 52.9 and 26.3 mm in the upper basin, respectively, 29.3, 38.4,

71.7 and 39.5 mm in the middle basin, and 39.6, 36.0, 95.7 and 46.3 mm in the lower basin, respectively.

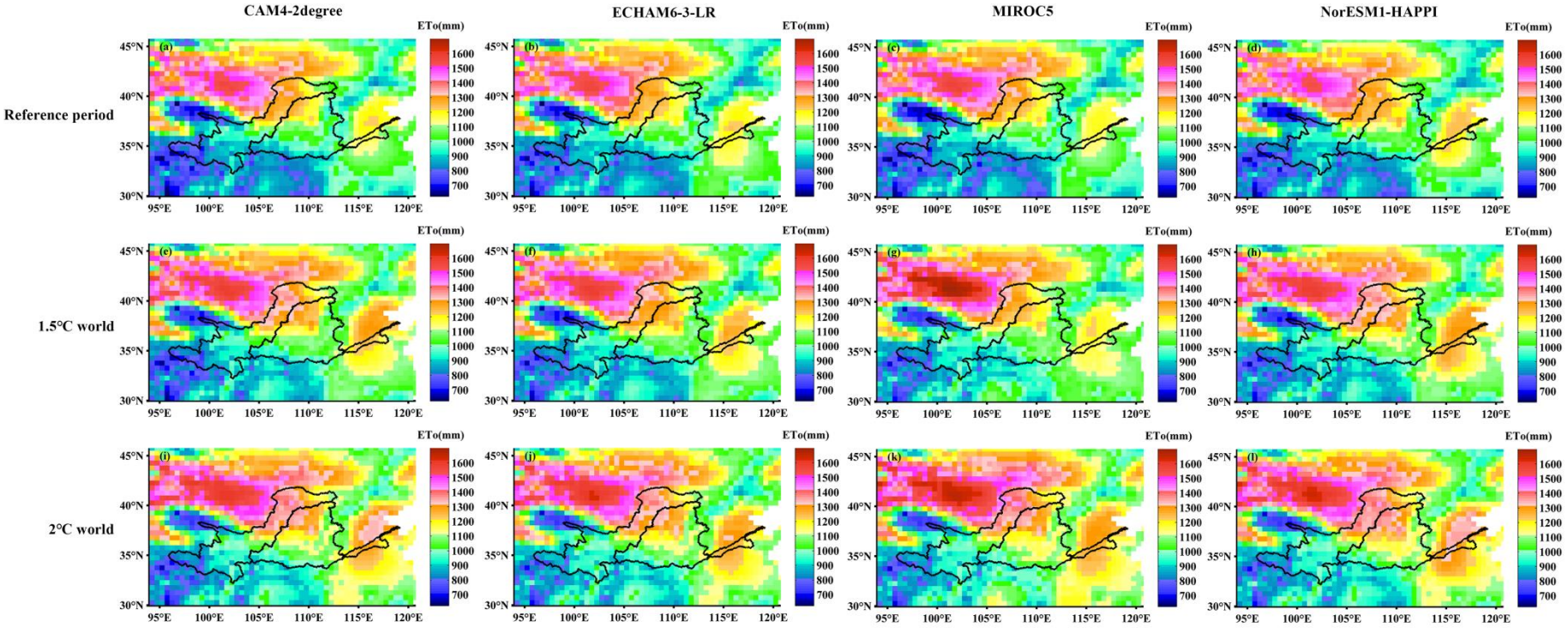

438 Fig. 8. Spatial distribution of ensemble mean ETo of mode at the reference period 1986 to 2005 (a, b, c, d) and at the 1.5°C (e, f, g, h) and 2°C warming levels (i, j,

439 k, l). The 1st, 2nd, 3rd, and 4th columns denotes ETo calculated by CAM4-2degree (a, e, i), ECHAM6-3-LR (b, f, j), MIROC5 (c, g, k) and NorESM1-HAPPI (d, h,

440 l), respectively.

441

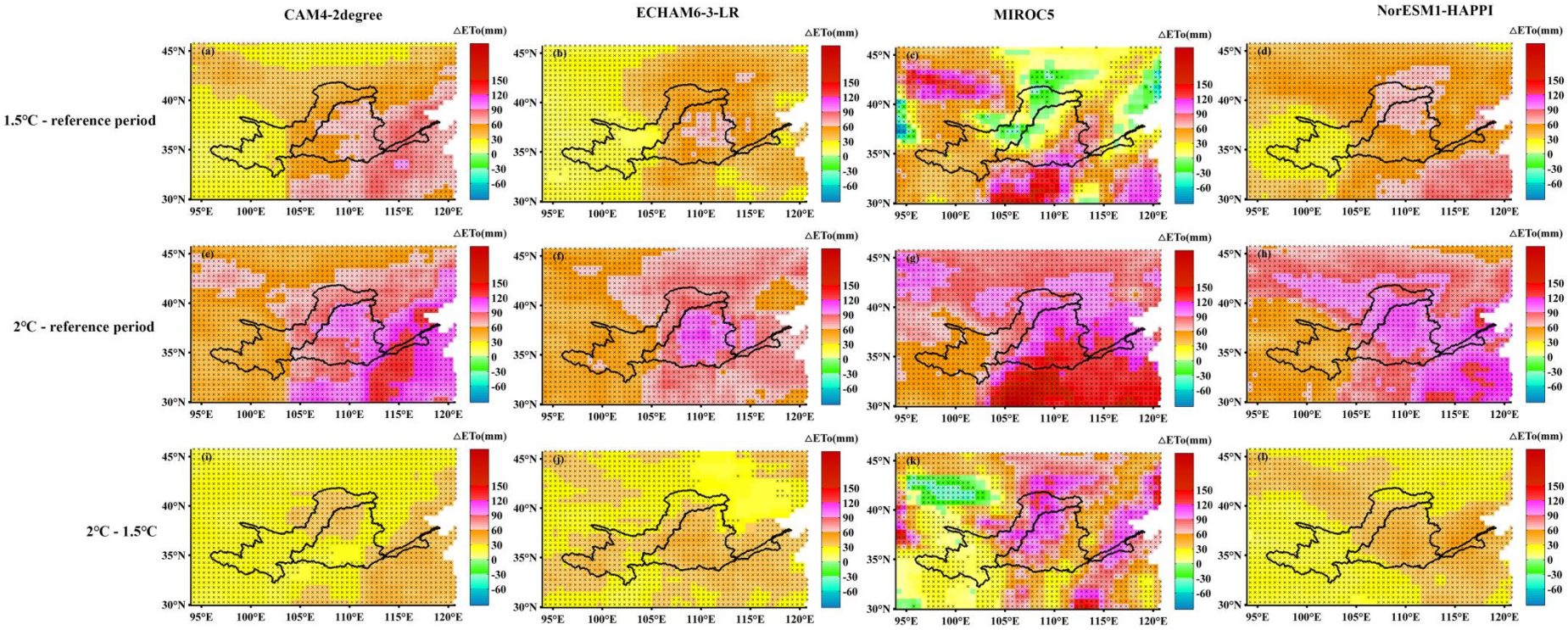

Fig. 9. Spatial distribution of changes in ensemble mean ETo of mode at the 1.5°C (a, b, c, d) and 2.0°C warming levels (e, f, g, h) with respect to the reference period of 2006-2015 and the difference in ETo between the 2 and 1.5°C warming levels (i, j, k, l). Hatchings are statistically significant at the 5% level according to a two-sided t test (95% confidence). The 1st, 2nd, 3rd, and 4th columns denote ETo calculated by CAM4-2degree (a, e, i), ECHAM6-3-LR (b, f, j), MIROC5 (c, g, k) and NorESM1-HAPPI (d, h, l), respectively.

The spatial distributions of the ETo for the reference period 2006 to 2015 and the 1.5 and 2.0°C warmer worlds are depicted in Fig. 8. Generally, the spatial patterns of the ETo among the four GCMs of HAPPI show similar characteristics in the 1.5 and 2°C warmer worlds to the reference period; however, the changes in the ETo in the different warming levels exhibit different spatial distributions among the different GCMs (Fig. 9). Generally, the ETo increases significantly in almost the whole YRB at the 1.5 and 2°C warming levels relative to the reference period for HAPPI. Specifically speaking, at a global warming of 1.5°C, the ETo increases most in the eastern region of the middle basin and lower basin for CAM4-2degree (>60 mm), the center of the middle basin for ECHAM6-3-LR (>60 mm), the southeastern region of the middle basin for MIROC5 (>60 mm) and northern parts of the upper and middle basins for NorESM1-HAPPI (>60 mm). The changes in ETo are relatively small in the upper basin for CAM4-2degree, ECHAM6-3-LR and NorESM1-HAPPI (<30 mm). For the MIROC5, the increment will be relatively small in the center of the upper basin and the western region of the middle basin (<30 mm), and the ETo even decreases in some areas of those regions.

For a 2°C warming world, the increment in the ETo is greater than 30 mm relative to the reference period. The spatial patterns of the increment of the ETo at the 2°C warming level with respect to the reference period are similar to those at 1.5°C, but the increment is greater and the ETo increases by more than 90 mm in most of the middle basin and lower basin for all GCMs.

The ETo increases significantly at the 2°C warming level compared to that at 1.5°C. There is a large increment in the ETo in the northern portion of the upper and middle basins and the lower basin, with an increment over 30 mm for CAM4-2degree and over 60 mm for MIROC5. The ETo increases by more than 30 mm in almost the whole basin for ECHAM6-3-LR and in the center of the upper basin and almost the whole middle and lower basins for NorESM1-HAPPI. Although the changes in the ETo between the two warming levels are diverse among GCMs, there is good consistency in that they are largest in the middle-northern area of the upper basin (southern part of Hetao Plain), the northwest of the middle basin (Ordos Plateau and northwest part of the Loess Plateau) and the lower basin (North China Plain).

3.5 Contribution of climatic variables to ETo change

The areal average of the contribution from a climatic variable to the change in the ETo for the whole, upper, middle and lower basins is listed in Tab. 3. The sum of the contributions from a single climatic variable to the ETo is unequal to the contribution from all variables (increment of ETo), but there is little difference between the two in most cases. The simple method was adopted to determine the relative contributions of the variables to the change of ETo. Broadly, the tasmax gives most positive contribution to the increase of ETo in the YRB at the 1.5 and 2°C warming levels, which is revealed by almost all GCMs. rsds also gives a certain positive contribution to the increase of the ETo at the two warming levels. An exception is that the main reason for the increase of the ETo projected by MIROC5 at

489 1.5°C warming is the rsds for the whole, middle and lower basins and the tmax for the
490 upper basin. Hurs gives some positive contribution to ETo projected by ECHAM6-3-
491 LR, which is greater than rsds at both warming levels. Specially, sfsWind has a great
492 negative effect on the increase of ETo at the 1.5°C warming level for MIROC5. All in
493 all, sfsWind and tmin make little contributions to the increase in ETo under global
494 warming of 1.5 and 2°C.

495 Tab. 3. Contributions of climatic variable to changes in ETo at 1.5 and 2°C warming levels

	496	CAM4-2degree				ECHAM6-3-LR				MIROC5				NorESM1-HAPPI			
		YRB	YRB_U	YRB_M	YRB_L	YRB	YRB_U	YRB_M	YRB_L	YRB	YRB_U	YRB_M	YRB_L	YRB	YRB_U	YRB_M	YRB_L
Global warming of 1.5°C	hurs	5.6	4.4	6.4	12.2	10.2	7.4	12.9	16.3	2.3	1.2	3.3	3.9	1.8	3	0.7	-1.9
	rsds	16.2	8.3	23.9	34	7.1	1.8	12.9	8.5	33.4	15.6	51.7	57.6	16.2	9.7	22.1	36.2
	sfsWind	0.9	-1.4	3	7.5	2.2	-0.8	5.4	4.4	-39.5	-32.3	-45.7	-64.7	-1	-3.5	1.5	3.2
	tmax	30.2	28.6	32	30.8	29.5	27.4	31.9	29.1	31.9	30.3	33.6	33.3	29.9	29.1	30.6	32.7
	tmin	1.7	2.3	2.3	0.1	3.1	3.3	3.3	4.6	5.1	5	5	7.3	3.3	4.1	4.1	0.6
	sum	54.7	42.2	67.7	84.6	52.1	39	66.4	62.8	33.2	19.9	47.8	37.4	50.1	42.4	59	70.8
	Increment of ETo	49.1	35.1	62.7	80.2	41.0	28.4	55.1	39.8	30.9	20.0	44.1	16.8	47.6	39.4	56.2	56.4
Global warming of 2°C	hurs	10.3	9.2	10.9	20.3	17.7	13	22.5	25.5	4	0.6	7.6	6.6	5.2	3.3	6.9	9.2
	rsds	18.3	8.9	27.4	39.7	10.5	4.4	17.3	11.7	30.6	13.3	48.3	53.5	20.3	11.2	28.6	45.9
	sfsWind	0.2	-2.6	2.7	8.4	3.1	-0.8	7.3	5.1	5.4	-0.4	10.8	22.7	-0.1	-3.4	3.5	1.9
	tmax	46.5	44.8	48	52	45.9	44.9	47.1	43.7	50.9	50.6	51.3	49.4	46.7	45.5	47.7	52.6
	tmin	7.0	7.9	7.9	5.4	9.7	9.6	9.6	12.7	12	12.1	12.1	14.6	9.8	10.3	10.3	7.5
	sum	82.3	68.2	96.8	125.8	86.9	71.1	103.8	98.6	102.9	76.2	130.1	146.8	81.9	66.9	97.1	117.1
	Increment of ETo	79.9	62.7	91.9	119.8	76.6	61.5	93.5	75.8	93.7	72.8	115.7	112.5	80.6	65.8	95.7	102.7

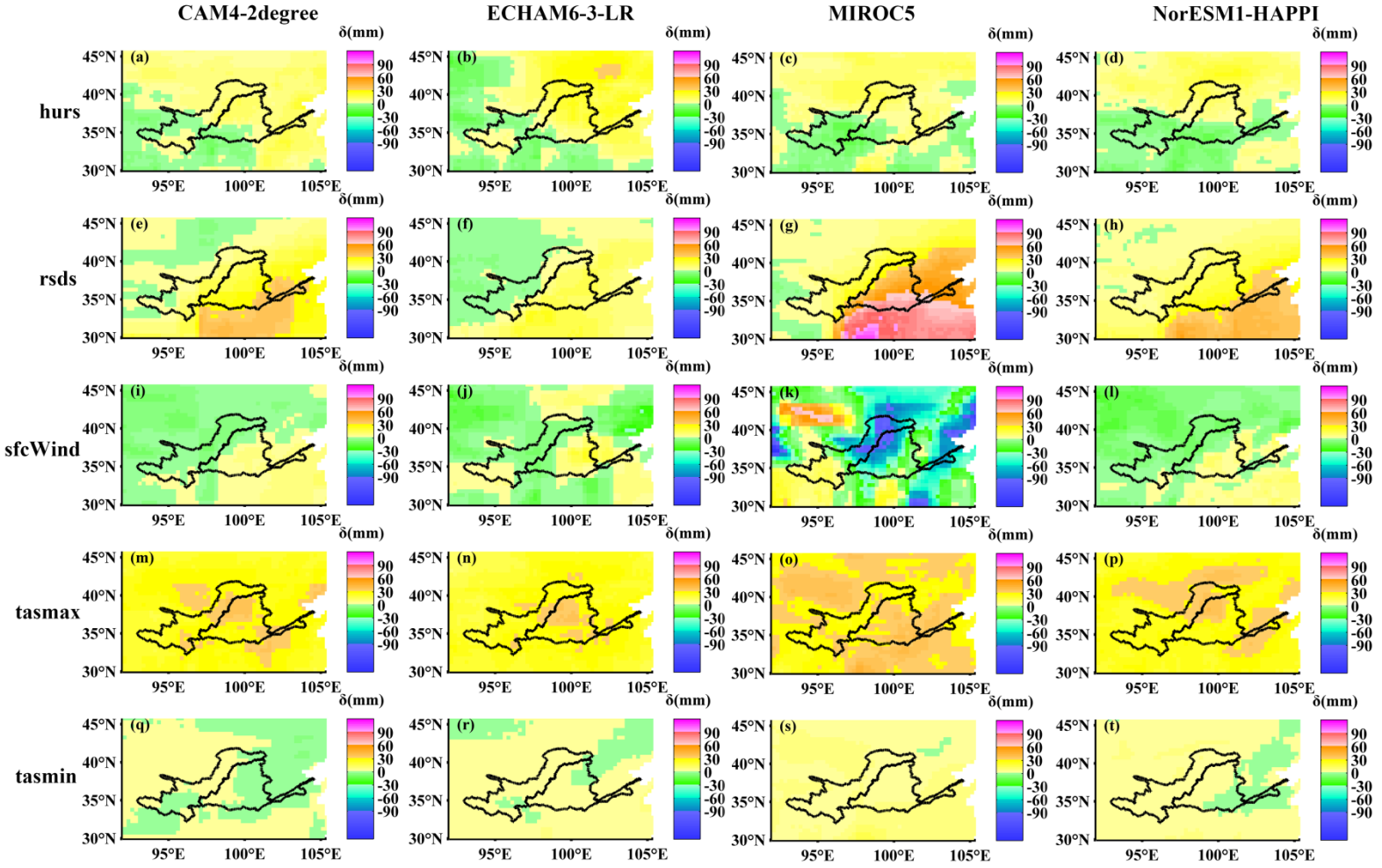
CAM4-2degree
ECHAM6-3-LR
MIROC5
NorESM1-HAPPI
hurs
rsds
sfcWind
tasmax
tasmin
δ(mm)
90
60
30
0
-30
-60
-90
45°N
40°N
35°N
30°N
95°E
100°E
105°E
(a)
(b)
(c)
(d)
(e)
(f)
(g)
(h)
(i)
(j)
(k)
(l)
(m)
(n)
(o)
(p)
(q)
(r)
(s)
(t)

Fig. 10. Spatial distribution of the contributions to the ETo change at the 1.5°C warming level. The 1st, 2nd, 3rd, 4th, and 5th rows indicates contributions of hurs (a, b, c, d), rsds (e, f, g, h), sfcWind (i, j, k, l), tmax (m, n, o, p), and tmin (q, r, s, t), respectively. The 1st, 2nd, 3rd, and 4th columns denote contributions for CAM4-2degree (a, e, i, m, q), ECHAM6-3-LR (b, f, j, n, r), MIROC5 (c, g, k, o, s) and NorESM1-HAPPI (d, h, l, p, t), respectively.

The spatial distributions of the contribution from a climatic variable to the change of the ETo at global warming of 1.5 and 2°C are shown in Fig. 10 and Fig. 11, respectively. At the 1.5°C warming level, the change in hurs has a negative effect on ETo at the southern part of the YRB and a positive effect at the northern part of the YRB. The change of rsds leads to an increase in the ETo in the whole basin for 4GCMs, except that it causes a decrease in ETo at the southern part of the upper basin for ECHAM6-3-LR. The change of sfcWind has a positive contribution to ETo in most of the middle and lower basins for CAM4-2degree, ECHAM6-3-LR and NorESM1-HAPPI. It induces an increase in ETo only at the southern portion of the upper basin for MIROC5. The tasmax gives a different level of increase in the ETo in the whole basin for all GCMs. The change of the tasmin has a positive contribution to the increase in ETo in most of the area of the YRB projected by HAPPI. It gives a negative contribution to ETo in the southern portion of the upper basin, eastern part of the middle basin and the lower basin for CAM4-2degree and at the eastern corner of the middle basin and the lower basin for NorESM1-HAPPI.

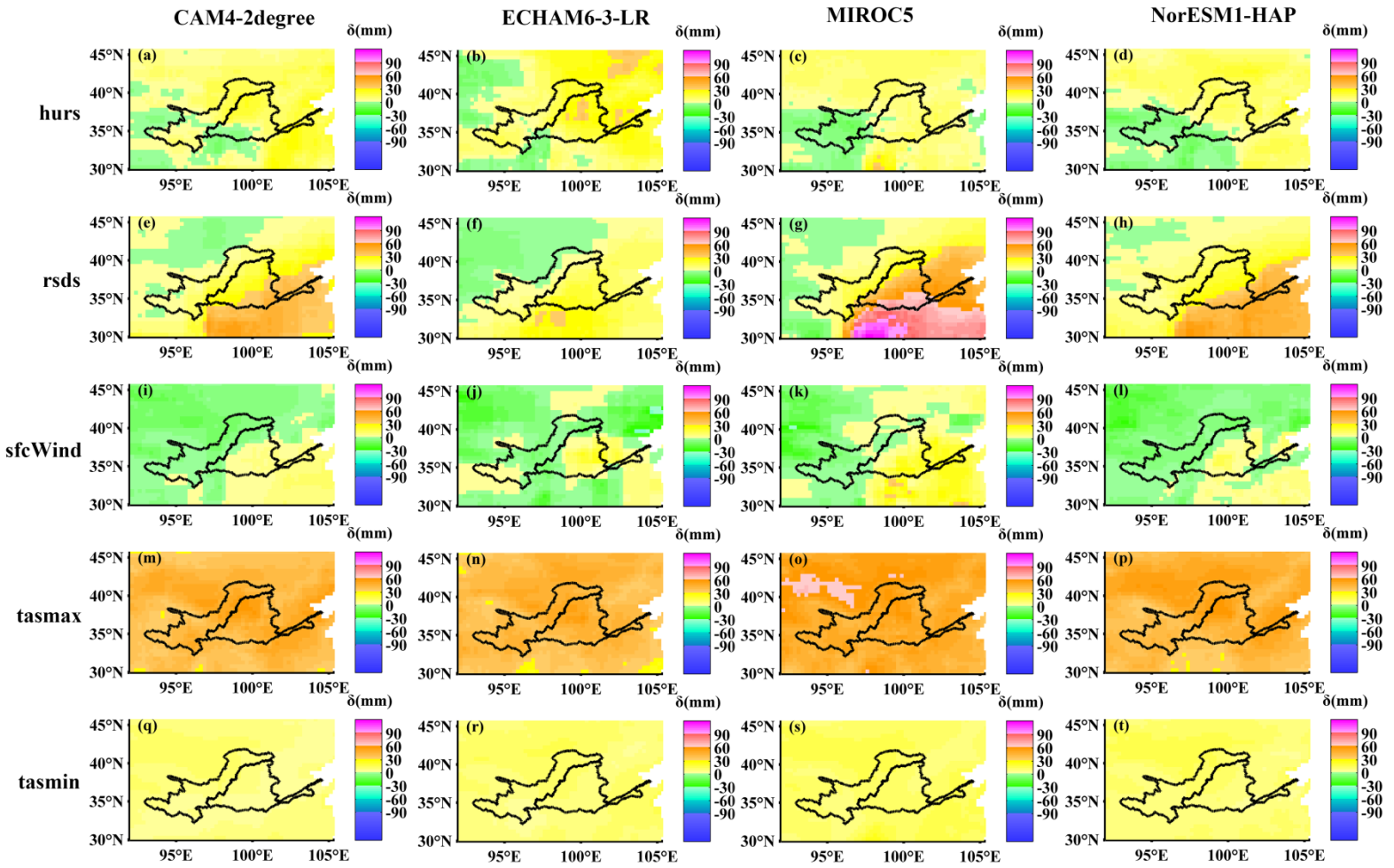

Fig. 11. As in Fig. 10, but for the 2°C warming level.

At the 2°C warming level, the contribution of the climatic variables has good consistency among the GCMs of HAPPI. The change of the hurs causes an increase of the ETo in the whole YRB for CAM4-2degree and ECHAM6-3-LR, and it gives rise to a decrease of ETo in the southern region of the upper basin and an increase of the ETo in the northern part of the upper basin and in the middle and lower basins for MIROC5 and NorESM1-HAPPI. The changes of the rsds, tasmax and tasmin make a positive contribution to the ETo in the entire YRB for all GCMs. The sfcWind still gives a negative contribution to the decrease of the ETo in the upper basin and western edge of the middle basin for all GCMs, and it gives a positive contribution at the central and eastern portions of the middle basin. It induces an increase in the ETo at the lower basin for CAM4-2degree, ECHAM6-3-LR and MIROC5 and a decrease of ETo for NorESM1-HAPPI.

4 Discussions

Tab. 4. Warming levels in the YRB during the 1.5 and 2.0 °C global warming above the pre-industrial level.

	Global warming of 1.5°C				Global warming of 2°C			
	CAM4-2degree	ECHAM6-3-LR	MIROC5	NorESM1-HAPPI	CAM4-2degree	ECHAM6-3-LR	MIROC5	NorESM1-HAPPI
YRB	1.62	1.66	1.98	1.79	2.27	2.33	2.64	2.51
YRB_U	1.57	1.64	1.92	1.77	2.25	2.32	2.65	2.49
YRB_M	1.67	1.69	2.06	1.81	2.3	2.34	2.65	2.54
YRB_L	1.65	1.58	1.96	1.65	2.26	2.23	2.43	2.31

534 Tab. 5. Changes of the precipitation in the YRB during the 1.5 and 2.0 °C global warming
535 compared to the reference period.

	Global warming of 1.5°C				Global warming of 2°C			
	CAM4-2degree	ECHAM6-3-LR	MIROC5	NorESM1-HAPPI	CAM4-2degree	ECHAM6-3-LR	MIROC5	NorESM1-HAPPI
YRB	9.98	-6.28	54.51	39.99	19.45	-12.59	61.12	40.81
YRB_U	12.55	-4.78	23.3	31.19	17.61	-11.8	29.91	41.08
YRB_M	7.35	-7.4	83.5	47.66	21.01	-13.24	89.26	39.37
YRB_L	6.48	-14.64	140.23	71.65	26.61	-16.03	159.6	57.71

536 Changes of the mean temperature compared to the pre-industrial level and
537 changes of the precipitation compared to the reference period at the 1.5 and 2.0 °C
538 global warming in the YRB are listed in Tab. 4 and 5, respectively. The global mean
539 surface temperature for the period of 2006–2015 was 0.87°C higher than the average
540 over the 1850–1900 period (IPCC, 2018). The warming above the pre-industrial level
541 in the YRB during the 1.5 and 2.0 °C global warming levels is the increment of the
542 mean temperature at the 1.5 and 2.0°C warming relative to the reference period plus
543 0.87°C, respectively. At the 1.5 and 2°C warmings, the whole YRB is warmer than
544 during pre-industrial times, particularly for the middle basin, where the warming level
545 is higher than in the other regions. The precipitation shows increasing trends for
546 CAM4-2degree, MIROC5, NorESM1-HAPPI in a 1.5 and 2°C warming world
547 compared to the reference period. The precipitation values at 2°C warming are greater
548 than at 1.5°C warming for CAM4-2degree and MIROC5. The precipitation projected
549 by NorESM1-HAPPI at the 2°C warming level is higher for the whole and upper
550 basins and lower for the middle and lower basins than at the 1.5°C warming level.
551 The precipitation projected by ECHAM6-3-LR both at 1.5 and 2°C warming shows

552 decreasing trends, and it decreases more at 2°C warming than at 1.5°C warming. All
553 in all, given the increase of the air temperature and precipitation, we are interested in
554 whether YRB will have dry or wet conditions.

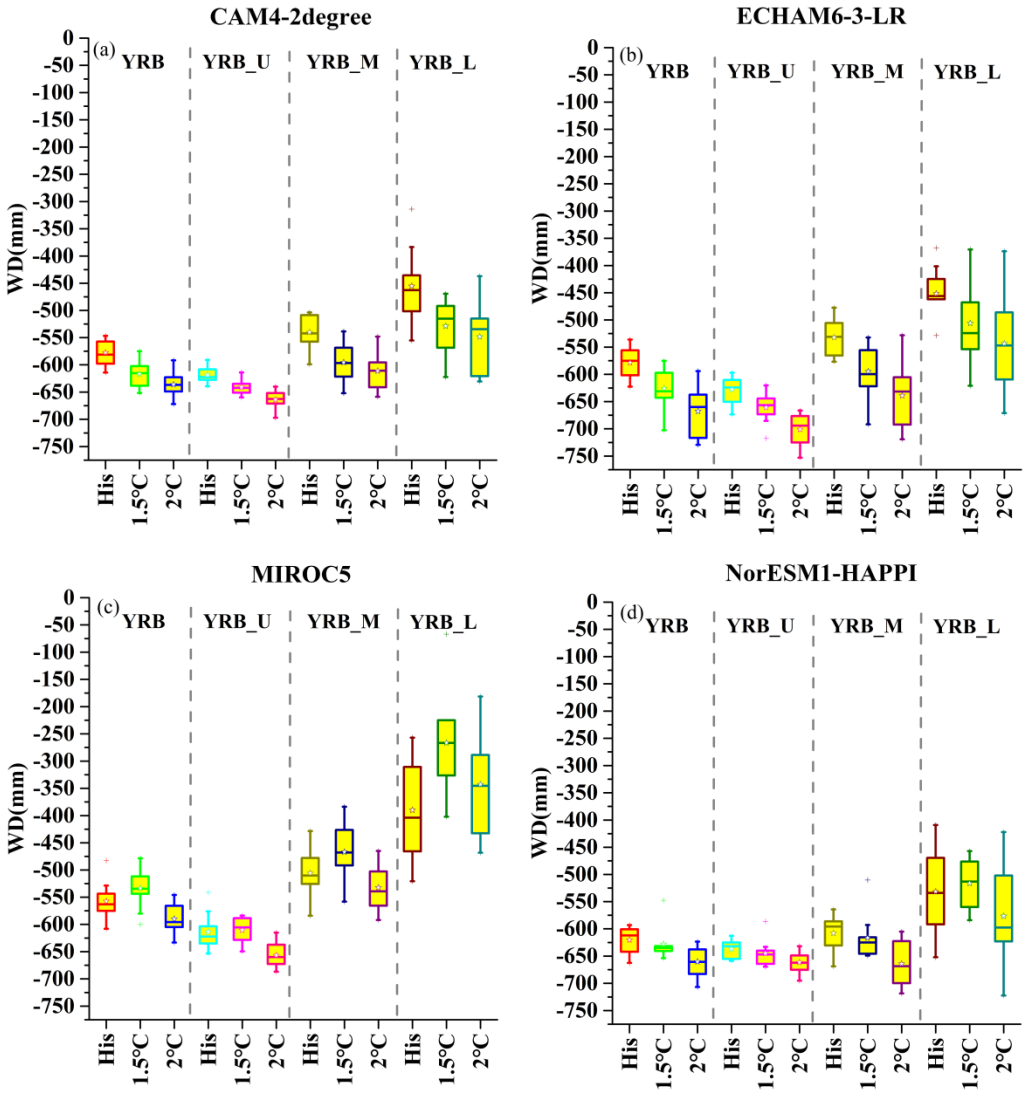

555

556 Fig. 12. Comparison of ensemble mean WD of mode in the whole (YRB), upper (YRB_U), middle
557 (YRB_M) and lower (YRB_L) basins during the reference period from 2006 to 2015 and under
558 global warming of 1.5°C and 2.0°C for (a) CAM4-2degree, (b) ECHAM6-3-LR, (c) MIROC5, (d)
559 NorESM1-HAPPI.

560 The climatic water deficit (WD, difference between the precipitation and ETo)
561 is calculated for the reference period and the 1.5 and 2°C global warming level. It can
562 be seen as an aridity index that can accurately quantify the water supply needed for a
563 reference crop (Paltineanu et al., 2007, 2009). It provides a simple measure of the
564 water surplus or deficit (Vicente-Serrano, Sergio et al., 2010). Boxplots of the annual
565 WD for the whole, upper, middle and lower basins are presented in Fig. 12. Except for
566 MIROC5, the WD under the three GCMs show decreasing trends at two warming
567 levels compared to the reference period. At 2°C warming, the WDs projected by all
568 four GCMs generally have more serious decreases in the whole basin. Generally, WD
569 has a greater decrease in the middle and lower basins. The WD presents an increasing
570 trend for MIROC5 at the 1.5°C warming level due to the projected increase in
571 precipitation; however, it decreases with the additional 0.5°C warming. As a
572 consequence, the YRB may experience drier conditions in a warmer world, and it is
573 more serious at the 2°C warming level.
574

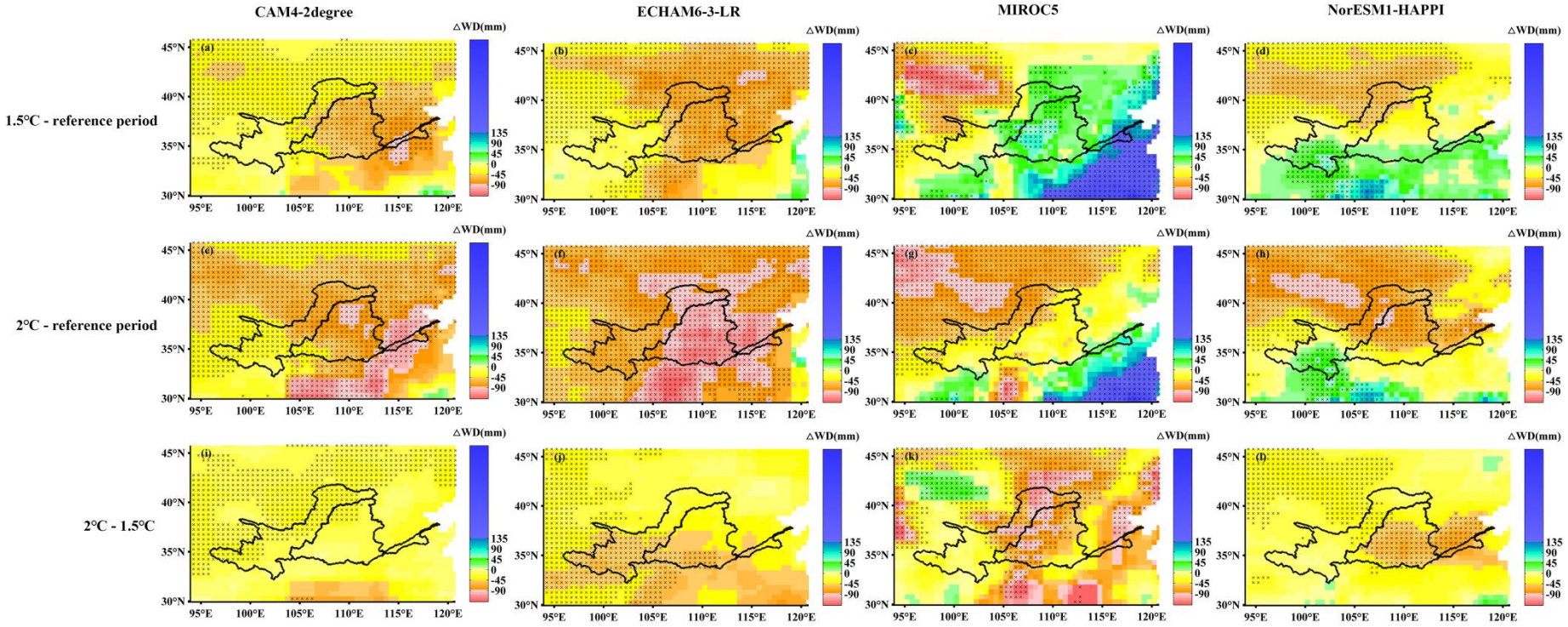

Fig. 13. As in Fig. 9, but for WD.

Fig. 13 shows the *changes* of the spatial patterns instead of the *absolute* spatial patterns of WD at different periods and shows that a majority of the YRB is characterized by decreasing trends in the WD at two warming levels projected by HAPPI, except for MIROC5. The WD decreases more in the 2°C warmer world in the entire basin by all GCMs of HAPPI. The increment of the ETo exceeds the increment of the precipitation, causing drier conditions in most area of YRB. On account of the great increase in precipitation at 1.5°C warming in the middle and lower basins projected by MIROC5 and in the south of YRB projected by NorESM1-HAPPI, these regions become wetter. The spatial patterns of change in WD are varied from GCMs, however, all GCMs give a consistent result that an additional 0.5°C warming will make almost the whole YRB drier.

Some researchers have analyzed the impact factors of the ETo in the YRB during the observed period by the contribution estimation method or sensitivity analysis method and found that the impact factors of changing in ETo varied spatially. Liu et al., (2010) revealed that there was a high sensitivity coefficient for ETo from 1961 to 2006 for the solar radiation for the upper basin, the wind speed for the northwest portion of the middle basin, relative humidity for the south portion of YRB and air temperature for the west portion of the upper basin and the north portion of the middle basin. Wang et al., (2012) discovered that the dominant factor for the decline in the ETo during 1957-2008 was a decrease in the wind speed in the west and north of the Loess Plateau and reduced sunshine duration in the middle-lower Yellow River Plain, while the dominant factor for the increase of ETo was an increasing mean temperature in the source area of the YRB. Our results revealed that the tasmax and rsds are the major driving forces for the increase of ETo at the 1.5 and 2°C warming levels and that the impact factors have good spatial consistency. It is likely that our results are different from the historical period because of

601 the changes in the climatic environment. The impact factor of ETo may change in a warmer
602 world, and the dominant factor is the maximum temperature. Contrary to the "evaporate
603 paradox", ETo does not show a decreasing trend with the climate warming, it increases
604 significantly, which may change the climatic environment of the YRB.

605 Our findings are supported by previous studies. Li et al. (2012) found that HadCM3
606 projects a continuous increase of ETo during the 21st century on the Loess Plateau. ETo will
607 increase by approximately 4%, 7% and 12% for the three periods 2011-2040, 2041-2070 and
608 2071-2099, respectively. Su et al. (2018) revealed that 13 global climate models (GCMs) in the
609 CMIP5 project significant increases in the ETo throughout China for both target periods.
610 Although the first above result does not consider 1.5 and 2°C warming, our consistent finding is
611 that the ETo might increase in the warmer world. A major limitation of this study is the
612 uncertainty of the results. In section 3.3, we evaluated HAPPI's simulations of the multiyear
613 averaged ETo and spatial pattern of the ETo. Although the GCMs give a minor error on the areal
614 averaged ETo and prominent performance on the spatial distribution of the ETo, their
615 simulations are larger than the ETo estimated by obsevered data. They show a large bias over
616 100 mm in the lower basin, northern part of the upper basin and northwestern portion of the
617 middle basin. Downscaling methods can give a better simulation of realistic climate variables
618 (Zhang et al., 2016), and after bias correction and statistical disaggregation, the uncertainty can
619 be reduced with respect to the observation (Su et al., 2016). Moreover, some uncertainty might
620 arise from inter-GCMs of HAPPI. GCMs give a consistent increase of ETo under global
621 warming of 1.5 and 2°C, but the magnitude of the increase and its spatial pattern are diverse. It is
622 not easy to determine which GCM is better than others. We do not calculated ensemble

projections from multiple GCMs, which may smooth the differences among GCMs, preferring to provide the true results for each GCM.

5 Conclusions

In this study, we investigated the spatiotemporal distribution of ETo in the YRB during 1961–2017 based on observed data and projected the ETo under global warming of 1.5 and 2°C based on outputs from HAPPI. The relative contributions of the climatic variables to change in ETo were quantified to determine the causes of the change in ETo at two warming levels. We also discussed changes in the climatic water deficit (difference between the precipitation and ETo) to assess wet/dry variations in the YRB in a warmer world. The following conclusions can be drawn from this study:

The ETo and ETo-trends exhibited spatial heterogeneity due to the complex spatial patterns during 1961-2017 in the YRB, and the ETo increased significantly for the upper basin (0.5 mm yr^{-1}) and decreased significantly for the middle (-0.23 mm yr^{-1}) and lower (-1.04 mm yr^{-1}) basins. The ETo value was the highest in the northern region of the upper basin (>1100 mm), followed by the eastern region of the middle basin and the lower basin (1000-1100 mm), the center of the upper basin and western region of the middle basin (900-1000 mm) and the southern part of the upper basin (<900 mm). Furthermore, the ETo increased significantly in the central and southern portions of the upper basin and the western portion of the middle basin, and it decreased significantly in a small part of the northeastern portion of the upper basin, the eastern portion of the middle basin and the lower basin.

HAPPI gave excellent simulations of the annual averages of ETo and spatial patterns of ETo in the reference period (2006-2015) in the YRB. There is a small bias for the higher ETo in

the northern portion of the upper and middle basins and the lower basin and a lower ETo in the southwestern portion of the upper basin and southern portion of the middle basin.

The multiyear average ETo of the YRB projected by CAM4-2degree, ECHAM6-3-LR, MIROC5 and NorESM1-HAPPI increases by 49.1, 41.0, 30.9 and 47.6 mm for a 1.5°C warmer world, respectively, and 77.9, 76.6, 93.7 and 80.6 mm for a 2°C warmer world, respectively, compared to compared to in the reference period. The ETo increases the most in the lower basin at both warming levels, follow by middle and upper basins. The increment in the ETo exceeds the increment of the precipitation in a warmer world and this may intensify the aridity of YRB. Limiting global warming to 1.5°C is beneficial to YRB for the lesser ETo and aridity. HAPPI gives a consistent projection that the ETo will decrease over 30mm in the lower basin (North China Plain), middle-northern area of the upper basin (southern part of Hetao Plain) and northwestern are of the middle basin (Ordos Plateau and northwestern part of the Loess Plateau) by limiting global warming to 1.5°C.

In a warmer world, tasmax has the greatest effect on the increase of ETo, and the causes of the increase in ETo at the 1.5 and 2°C warming levels have good spatial consistancy. rsds and hurs also have contributions to the increase in ETo. sfsWind and tasmin have smaller contributions to the increase of ETo.

Acknowledgments

This study is jointly sponsored by the National Key R&D Program of China (2016YFA0600404), the National Natural Science Foundation of China (41530532), the China Special Fund for Meteorological Research in the Public Interest (GYHY201106028), and the Jiangsu Collaborative Innovation Center for Climate Change. We acknowledge the HAPPI core

team and NERSC for data storage. DMM was supported by a NERC independent research fellowship (NW/N014057/1).

Reference

Allen, R. G., Pereira, L. S., Raes, D., & Smith, M. (1998). Crop evapotranspiration—Guidelines for computing crop water requirements. FAO Irrigation and Drainage Paper 56, Rome, Italy. Retrieved from https://appgeodb.nancy.inra.fr/biljou/pdf/Allen_FAO1998.pdf

Baker, H. S., Millar, R. J., Karoly, D. J., Beyerle, U., Guillod, B. P., Mitchell, D., et al. (2018). Higher CO2 concentrations increase extreme event risk in a 1.5 °C world. *Nature Climate Change*, 8(7), 604-608. https://doi.org/10.1038/s41558-018-0190-1

Bandyopadhyay, A., Bhadra, A., Raghuwanshi, N. S., & Singh, R. (2009). Temporal Trends in Estimates of Reference Evapotranspiration over India. *Journal of Hydrologic Engineering*, 14(5), 508-515. https://doi.org/10.1061/(ASCE)HE.1943-5584.0000006

Burn, D. H., & Hesch, N. M. (2007). Trends in evaporation for the Canadian Prairies. *Journal of Hydrology*, 336(1), 61-73. https://doi.org/ 10.1016/j.jhydrol.2006.12.011

Cai, X., & Rosegrant, M. W. (2004). Optional water development strategies for the Yellow River Basin: Balancing agricultural and ecological water demands. *Water Resources Research*, 40(8). https://doi.org/doi:10.1029/2003WR002488

Chattopadhyay, N., & Hulme, M. (1997). Evaporation and potential evapotranspiration in India under conditions of recent and future climate change. *Agricultural and Forest Meteorology*, 87(1), 55-73. https://doi.org/ 10.1016/S0168-1923(97)00006-3

Cong, Z., Yang, D., Gao, B., Yang, H., & Hu, H. (2009). Hydrological trend analysis in the Yellow River basin using a distributed hydrological model. *Water Resources Researc*h, 45(7). https://doi.org/doi:10.1029/2008WR006852

Cuo, L., Zhang, Y., Gao, Y., Hao, Z., & Cairang, L. (2013). The impacts of climate change and land cover/use transition on the hydrology in the upper Yellow River Basin, China. *Journal of Hydrology*, 502, 37-52. https://doi.org/ /10.1016/j.jhydrol.2013.08.003

693 Döll, P., Trautmann, T., Gerten, D., Schmied, H. M., Ostberg, S., Saaed, F., & Schleussner, C.-F. (2018). Risks for
694 the global freshwater system at 1.5 °C and 2 °C global warming. Environmental Research Letters, 13(4),
695 044038. https://doi.org/10.1088/1748-9326/aab792
696 Douglas, I. (1989). Land degradation, soil conservation and the sediment load of the Yellow River, China:
697 Review and assessment. Land Degradation & Development, 1(2), 141-151.
698 https://doi.org/doi:10.1002/ldr.3400010206
699 Fu, G., Chen, S., Liu, C., & Shepard, D. (2004). Hydro-Climatic Trends of the Yellow River Basin for the Last
700 50 Years. *Climatic Change*, 65(1), 149-178. https://doi.org/10.1023/B:CLIM.0000037491.95395.bb
701 Golubev, V. S., Lawrimore, J. H., Groisman, P. Y., Speranskaya, N. A., Zhuravin, S. A., Menne, M. J., et al.
702 (2001). Evaporation changes over the contiguous United States and the former USSR: A reassessment.
703 *Geophysical Research Letters*, 28(13), 2665-2668. https://doi.org/doi:10.1029/2000GL012851
704 Gong, L., Xu, C.-y., Chen, D., Halldin, S., & Chen, Y. D. (2006). Sensitivity of the Penman–Monteith
705 reference evapotranspiration to key climatic variables in the Changjiang (Yangtze River) basin. *Journal of*
706 *Hydrology*, 329(3), 620-629. https://doi.org/10.1016/j.jhydrol.2006.03.027
707 Hobbins, M. T. (2004). Regional evapotranspiration and pan evaporation: Complementary interactions and
708 long-term trends across the Conterminous United States (Doctoral dissertation), Fort Collins, CO:
709 Colorado State University.
710 IPCC, 2018: *Summary for Policymakers. In: Global warming of 1.5°C. An IPCC Special Report on the*
711 *impacts of global warming of 1.5°C above pre-industrial levels and related global greenhouse gas*
712 *emission pathways, in the context of strengthening the global response to the threat of climate change,*
713 *sustainable development, and efforts to eradicate poverty* [V. Masson-Delmotte, P. Zhai, H. O. Pörtner,
714 D. Roberts, J. Skea, P. R. Shukla, A. Pirani, W. Moufouma-Okia, C. Péan, R. Pidcock, S. Connors, J. B.
715 R. Matthews, Y. Chen, X. Zhou, M. I. Gomis, E. Lonnoy, T. Maycock, M. Tignor, T. Waterfield (eds.)].
716 World Meteorological Organization, Geneva, Switzerland, 32 pp.
717 Jhajharia, D., Shrivastava, S. K., Sarkar, D., & Sarkar, S. (2009). Temporal characteristics of pan evaporation
718 trends under the humid conditions of northeast India. *Agricultural and Forest Meteorology*, 149(5), 763-
719 770. https://doi.org/10.1016/j.agrformet.2008.10.024

Jian, D., Li, X., Sun, H., Tao, H., Jiang, T., Su, B., & Hartmann, H. (2018). Estimation of Actual Evapotranspiration by the Complementary Theory-Based Advection–Aridity Model in the Tarim River Basin, China. *Journal of Hydrometeorology*, 19(2), 289-303. https://doi.org/10.1175/jhm-d-16-0189.1

Jun, A., Hideyukin K., & Lu M. (2004). Pan evaporation trends in Japan and its relevance to the variability of the hydrological cycle. *Tenki*, 51(9), 667–678.

Kendall, M. G. (1975). *Rank correlation methods*. New York: Oxford University Press.

Lange, S. 2018. Bias correction of surface downwelling longwave and shortwave radiation for the EWEMBI dataset. *Earth System Dynamics*. 9, 627–645. https://doi.org/10.5194/esd-9-627-2018

Lewis, S. C., King, A. D., & Mitchell, D. M. (2017). Australia's Unprecedented Future Temperature Extremes Under Paris Limits to Warming. *Geophysical Research Letters*, 44(19), 9947-9956. https://doi.org/doi:10.1002/2017GL074612

Li, Z., Zheng, F. L., & Liu, W. Z. (2012). Spatiotemporal characteristics of reference evapotranspiration during 1961–2009 and its projected changes during 2011–2099 on the Loess Plateau of China. *Agricultural and Forest Meteorology*, 154–155, 147-155. http://dx.doi.org/10.1016/j.agrformet.2011.10.019

Liu, B., Xu, M., Henderson, M., & Gong, W. (2004). A spatial analysis of pan evaporation trends in China, 1955–2000. *Journal of Geophysical Research: Atmospheres*, 109(D15). https://doi.org/doi:10.1029/2004JD004511

Liu, Q., Yang, Z., Cui, B., & Sun, T. (2010). The temporal trends of reference evapotranspiration and its sensitivity to key meteorological variables in the Yellow River Basin, China. Hydrological Processes, 24(15), 2171-2181. https://doi.org/doi:10.1002/hyp.7649

Lv, M., Ma, Z., Yuan, X., Lv, M., Li, M., & Zheng, Z. (2017). Water budget closure based on GRACE measurements and reconstructed evapotranspiration using GLDAS and water use data for two large densely-populated mid-latitude basins. Journal of Hydrology, 547, 585-599. https://doi.org/10.1016/j.jhydrol.2017.02.027

Lv, M. X., Ma, Z. G., Lv, M. Z. (2018). Effects of climate/land surface changes on streamflow with consideration of precipitation intensity and catchment characteristics in the yellow river basin. *Journal of Geophysical Research: Atmospheres*, 123(4), 1942-1958. https://doi.org/doi:10.1002/2017JD027625

Ma, Z. G. (2005). Historical regular patterns of the discharge in the Yellow River and the cause of their formation (in Chinese). *Chinese Journal of Geophysics*, 48(6), 1270-1275. https://doi.org/10.3321/j.issn:0001-5733.2005.06.007

Mann, H. B. (1945). Nonparametric tests against trend. *Econometrica: Journal of the Econometric Society*, 13(3), 245–259. https://doi.org/ 10.2307/1907187

McVicar, T. R., Li, L., Van Niel, T. G., Zhang, L., Li, R., Yang, Q., et al. (2007). Developing a decision support tool for China's re-vegetation program: Simulating regional impacts of afforestation on average annual streamflow in the Loess Plateau. *Forest Ecology and Management*, 251(1), 65-81. https://doi.org/10.1016/j.foreco.2007.06.025

Mitchell, D., AchutaRao, K., Allen, M., Bethke, I., Beyerle, U., Ciavarella, A., et al. (2017). Half a degree additional warming, prognosis and projected impacts (HAPPI): background and experimental design. *Geoscientific Model Development*, 10(2), 571-583. https://doi.org/10.5194/gmd-10-571-2017

Mitchell, D., James, R., Forster, P. M., Betts, R. A., Shiogama, H., & Allen, M. (2016). Realizing the impacts of a 1.5 [deg]C warmer world. *Nature Climate Change*, 6(8), 735-737. https://doi.org/10.1038/nclimate3055

Paltineanu, C., Mihailescu, I. F., Prefac, Z., Dragota, C., Vasenciuc, F., & Claudia, N. (2008). Combining the standardized precipitation index and climatic water deficit in characterizing droughts: a case study in Romania. *Theoretical and Applied Climatology*, 97(3-4), 219-233. https://doi.org/10.1007/s00704-008-0061-1

Paltineanu, C., Mihailescu, I. F., Seceleanu, I., Dragota, C., & Vasenciuc, F. (2007). Using aridity indices to describe some climate and soil features in Eastern Europe: a Romanian case study. *Theoretical and Applied Climatology*, 90(3-4), 263-274. https://doi.org/10.1007/s00704-007-0295-3

Peterson, T. C., Golubev, V. S., & Groisman, P. Y. (1995). Evaporation losing its strength. *Nature*, 377, 687. https://doi.org/10.1038/377687b0

Roderick, M. L., & Farquhar, G. D. (2002). The Cause of Decreased Pan Evaporation over the Past 50 Years. *Science*, 298(5597), 1410-1411. https://doi.org/10.1126/science.1075390-a

773 Roderick, M. L., & Farquhar, G. D. (2004). Changes in Australian pan evaporation from 1970 to 2002.
774 *International Journal of Climatology*, 24(9), 1077-1090. https://doi.org/10.1002/joc.1061
775 Roderick, M. L., Rotstayn, L. D., Farquhar, G. D., & Hobbins, M. T. (2007). On the attribution of changing
776 pan evaporation. *Geophysical Research Letter*s, 34(17). https://doi.org/10.1029/2007GL031166
777 Ruane, A. C., Phillips, M. M., & Rosenzweig, C. (2018). Climate shifts within major agricultural seasons for
778 +1.5 and +2.0 °C worlds: HAPPI projections and AgMIP modeling scenarios. *Agricultural and Forest*
779 *Meteorology*, 259, 329-344. https://doi.org/10.1016/j.agrformet.2018.05.013
780 Schleussner, C. F., Deryng, D., Müller, C., Elliott, J., Saeed, F., Folberth, C., et al. (2018). Crop productivity
781 changes in 1.5 °C and 2 °C worlds under climate sensitivity uncertainty. *Environmental Research Letters*,
782 13(6), 064007. https://doi.org/10.1088/1748-9326/aab63b
783 Schleussner, C. F., Rogelj, J., Schaeffer, M., Lissner, T., Licker, R., Fischer, E. M., et al. (2016). Science and
784 policy characteristics of the Paris Agreement temperature goal. *Nature Climate Change*, 6(9), 827-835.
785 https://doi.org/10.1038/nclimate3096
786 Seneviratne, S. I., Wartenburger, R., Guillod, B. P., Hirsch, A. L., Vogel, M. M., Brovkin, V., et al. (2018).
787 Climate extremes, land–climate feedbacks and land-use forcing at 1.5°C. Philosophical Transactions of
788 the Royal Society A: Mathematical, *Physical and Engineering Sciences*, 376(2119).
789 https://doi.org/10.1098/rsta.2016.0450
790 She, D., & Xia, J. (2013). The spatial and temporal analysis of dry spells in the Yellow River basin, China.
791 *Stochastic Environmental Research and Risk Assessment*, 27(1), 29-42. https://doi.org/10.1007/s00477-
792 011-0553-x
793 Shi, H., & Shao, M. (2000). Soil and water loss from the Loess Plateau in China. *Journal of Arid*
794 *Environments*, 45(1), 9-20. https://doi.org/10.1006/jare.1999.0618
795 Shiau, J. T., Feng, S., & Nadarajah, S. (2007). Assessment of hydrological droughts for the Yellow River,
796 China, using copulas. *Hydrological Processes*, 21(16), 2157-2163. https://doi.org/doi:10.1002/hyp.6400
797 Su, B., Huang, J., Fischer, T., Wang, Y., Kundzewicz, Z. W., Zhai, J., et al. (2018). Drought losses in China
798 might double between the 1.5 °C and 2.0 °C warming. *Proceedings of the National Academy of Sciences*.
799 https://doi.org/10.1073/pnas.1802129115

Su, B., Huang, J., Gemmer, M., Jian, D., Tao, H., Jiang, T., & Zhao, C. (2016). Statistical downscaling of CMIP5 multi-model ensemble for projected changes of climate in the Indus River Basin. *Atmospheric Research*, 178-179, 138-149. https://doi.org/10.1016/j.atmosres.2016.03.023

Su, B., Jian, D., Li, X., Wang, Y., Wang, A., Wen, S., et al. (2017). Projection of actual evapotranspiration using the COSMO-CLM regional climate model under global warming scenarios of 1.5°C and 2.0°C in the Tarim River basin, China. *Atmospheric Research*, 196, 119-128. https://doi.org/10.1016/j.atmosres.2017.06.015

Sun, Q., Miao, C., & Duan, Q. (2015). Projected changes in temperature and precipitation in ten river basins over China in 21st century. *International Journal of Climatology*, 35(6), 1125-1141. https://doi.org/doi:10.1002/joc.4043

Tang, K. L., Chen, Y. Z., & Jing, K. (1991). *Characteristics of soil erosion and its control on Loess Plateau (in Chinese).* Beijing: Science and technology of China press.

Taylor, K. E., Stouffer, R. J., & Meehl, G. A. (2012). An overview of CMIP5 and the experiment design. *Bulletin of the American Meteorological Society*, 93(4), 485-498. https://doi.org/10.1175/bams-d-11-00094.1

Trenberth, K. E., Dai, A., van der Schrier, G., Jones, P. D., Barichivich, J., Briffa, K. R., & Sheffield, J. (2013). Global warming and changes in drought. *Nature Climate Change*, 4, 17. https://doi.org/10.1038/nclimate2067

Vicente-Serrano, S. M., Beguería, S., & López-Moreno, J. I. (2009). A Multiscalar Drought Index Sensitive to Global Warming: The Standardized Precipitation Evapotranspiration Index. *Journal of Climat*e, 23(7), 1696-1718. https://doi.org/10.1175/2009JCLI2909.1

Vicente-Serrano, S. M., Beguería, S., Lorenzo-Lacruz, J., Camarero, J. J., López-Moreno, J. I., Azorin-Molina, C., et al. (2012). Performance of Drought Indices for Ecological, Agricultural, and Hydrological Applications. *Earth Interactions*, 16(10), 1-27. https://doi.org/10.1175/2012ei000434.1

Vicente-Serrano, S. M., Van der Schrier, G., Beguería, S., Azorin-Molina, C., & Lopez-Moreno, J.-I. (2015). Contribution of precipitation and reference evapotranspiration to drought indices under different climates. *Journal of Hydrology*, 526, 42-54. https://doi.org/https://doi.org/10.1016/j.jhydrol.2014.11.025

827 Wang, W., Shao, Q., Peng, S., Xing, W., Yang, T., Luo, Y., et al. (2012). Reference evapotranspiration change
828 and the causes across the Yellow River Basin during 1957–2008 and their spatial and seasonal
829 differences. *Water Resources Research*, 48(5). https://doi.org/doi:10.1029/2011WR010724
830 Wang, Y., & Peng, S.M. (Eds.). (2017). *Principle and technology of drought monitoring and water resource*
831 *allocation in the Yellow River basin* (in Chinese). Beijing: Science press.
832 Wang, Y., Ding, Y., Ye, B., Liu, F., Wang, J., & Wang, J. (2013). Contributions of climate and human
833 activities to changes in runoff of the Yellow and Yangtze rivers from 1950 to 2008. *Science China Earth*
834 *Sciences*, 56(8), 1398-1412. https://doi.org/10.1007/s11430-012-4505-1
835 Wang, Z., Xie, P., Lai, C., Chen, X., Wu, X., Zeng, Z., & Li, J. (2017). Spatiotemporal variability of reference
836 evapotranspiration and contributing climatic factors in China during 1961–2013. *Journal of Hydrology*,
837 544, 97-108. https://doi.org/10.1016/j.jhydrol.2016.11.021
838 Wehner, M., Stone, D., Mitchell, D., Shiogama, H., Fischer, E., Graff, L. S., et al. (2018). Changes in
839 extremely hot days under stabilized 1.5 and 2.0 °C global warming scenarios as simulated by the HAPPI
840 multi-model ensemble. *Earth System Dynamics*, 9(1), 299-311. https://doi.org/10.5194/esd-9-299-2018
841 Xie, Y. G., & Fu, Q. (2004). Analysis of famines caused by heavy floods and droughts in China. *Nature and*
842 *Science*, 2 (2), 25–32.
843 Xu, C., & Singh, V. P. (2004). Review on Regional Water Resources Assessment Models under Stationary and
844 Changing Climate. *Water Resources Management*, 18(6), 591-612. https://doi.org/10.1007/s11269-004-
845 9130-0
846 Xu, C., Gong, L., Jiang, T., Chen, D., & Singh, V. P. (2006). Analysis of spatial distribution and temporal
847 trend of reference evapotranspiration and pan evaporation in Changjiang (Yangtze River) catchment.
848 *Journal of Hydrology*, 327(1–2), 81-93. http://dx.doi.org/10.1016/j.jhydrol.2005.11.029
849 Yan, Y., Yang, Z., & Liu, Q. (2013). Nonlinear trend in streamflow and its response to climate change under
850 complex ecohydrological patterns in the Yellow River Basin, China. *Ecological Modelling*, 252, 220-227.
851 https://doi.org/10.1016/j.ecolmodel.2012.05.022

852 Yang, D., Li, C., Hu, H., Lei, Z., Yang, S., Kusuda, T., et al. (2004). Analysis of water resources variability in
853 the Yellow River of China during the last half century using historical data. *Water Resources Researc*h,
854 40(6). https://doi.org/doi:10.1029/2003WR002763
855 Yellow River Conservancy Commission of MWR (YRCC). (2007). *Yellow River water resources bulletin* (in
856 Chinese). Zhengzhou: Yellow River Conservancy Press.
857 Yellow River Conservancy Commission of MWR (YRCC). (2015). *Yellow River water resources bulletin* (in
858 Chinese). Zhengzhou: Yellow River Conservancy Press.
859 Zhai, R., Tao, F., & Xu, Z. (2018). Spatial–temporal changes in runoff and terrestrial ecosystem water
860 retention under 1.5 and 2 °C warming scenarios across China. *Earth System Dynamics*, 9(2), 717-738.
861 https://doi.org/10.5194/esd-9-717-2018
862 Zhang, Y., You, Q., Chen, C., & Ge, J. (2016). Impacts of climate change on streamflows under RCP
863 scenarios: A case study in Xin River Basin, China. *Atmospheric Research*, 178-179, 521-534.
864 https://doi.org/10.1016/j.atmosres.2016.04.018
865 Zhu, Z., Giordano, M., Cai, X., & Molden, D. (2004). The Yellow River Basin: Water Accounting, Water
866 Accounts, and Current Issues. Water International, 29(1), 2-10.
867 https://doi.org/10.1080/02508060408691742